Multilevel Nanoengineering for Imprint Lithography

Mark Konijn B.E. (Hons)

A thesis submitted in partial fulfilment
of the requirements for the degree of
Master of Engineering
in
Electrical and Electronic Engineering
at the
University of Canterbury,
Christchurch, New Zealand.

15 July 2005

ABSTRACT

Abstract The current trend in pushing photo lithography to smaller and smaller resolutions is becoming increasingly difficult and expensive. Extreme ultra-violet lithography is an alternate method that has the potential to provide feature sizes down to 30 nm, however, it will come at an even greater cost. Nanoimprint lithography (NIL) is another lithographic technique which is promising to provide very high resolutions at a relatively low cost. Imprinting works by using a mold with a surface patterned with the required nano structures and pressing it into a substrate coated with a deformable polymer. Due to its direct pattern replication technique, it is very capable of reproducing three-dimensional structures, however limited research has been performed on this to date.

In this study, investigations have been performed into developing a reliable process for creating Si_xN_y molds with sub-100 nm structures with variable height control. The process relies on a negative tone electron beam resist which can be patterned to various thicknesses by varying the exposure dosage. This allows for the creation of complex multi-layer structures in a single electron beam lithography step. These patterns then have been transferred into the Si_xN_y substrate by a single reactive ion etch. From here the mold is ready for use in imprinting.

Study has also been performed into imprinting process as well. This includes the development of an imprint press, the manner in which NIL works. Investigations have been performed into the imprinting performance of 3D molds. Thermal expansion issues have been found and addressed, as have adhesion problems. Some other aspects of 3D NIL which have not been addressed in this study have been outlined in future work for further investigation.

ACKNOWLEDGEMENTS

I must firstly acknowledge and thank my supervisor, Dr M. M. Alkaisi, for suggesting this thesis project on an interesting and new area of research, and for his help and guidance on nanoimprint technology. I must also thank my co-supervisor, Dr R. J. Blaikie, for advice on some difficult lithography issues.

I would like to acknowledge the MacDiarmid Institute for their financial support during my studies.

Special thanks must go to other academic staff at the university. They are: Dr J. Smail, for help on mechanical systems, Dr. A. Downard, for assistance with the chemistry of self assembling monolayers, and Dr S. Krumdieck, for an introduction to chemical vapour deposition systems.

Thanks must also be offered to the laboratory technicians, G. Turner and H. Devereux, who did their best to keep the laboratory clean and all equipment operational. Thanks must also go to other technical staff of D. Sallis, S. Downing, D. van Leeuwen, P. Kikstra, D. Berry, and R. Battersby who also helped in other means in areas outside of the laboratory.

I also wish to give thanks to R. Munro and M. Griffiths for their assistance with official paperwork.

Fellow students at the University of Canterbury must also be thanked for their technical (and otherwise) discussions. They are E. D. Walsby, V. Christie, S. J. Drake (for LaTeX help), J. Muys, D. Melville, G. Kanesan, W. Jayatissa, K. Mohamed, L. Schuler, the R9 Office crew of S. Hardie, P. Barclay, S. Fortune, E. Pilbrow, L. Frigidaire, and my flatmates over the years.

I would finally like to thank my family, Nick, Thea, Petra, Judith and Dennis, for their love and support throughout my study.

GLOSSARY

AFM	Atomic force microscope
CD	Compact disc
CVD	Chemical vapour Ddposition
DAC	Digital to analogue converter
DIW	De-ionised water
DUV	Deep ultra-violet
DVD	Digital versatile disc
EBL	Electron beam lithography
EUV	Extreme ultra-violet
FIB	Focused ion beam
FOTS	trichloro(1H,1H,2H,2H-perflouroctyl)silane - $(CF_3(CF_2)_5(CH_2)_2SiCl_3)$
HMDS	Hexamethyldisilazane
HMW	High molecular weight
IC	Integrated circuit
IPA	Isopropyl alcohol
IR	Infra-red
LMW	Low molecular weight
LPCVD	Low pressure chemical vapour deposition
MIBK	Methyl isobutyl ketone
NGL	Next generation lithography
NIL	Nanoimprint lithography
PDMS	Poly(dimethylsiloxane)
PMMA	Poly(methyl methacrylate)
RF	Radio frequency
RIE	Reactive ion etching
RPM	Revolutions per minute
SEM	Scanning electron microscope
SFIL	Step and flash imprint lithography
UV	Ultra-violet
UoC	University of Canterbury

CONTENTS

LIST OF FIGURES

LIST OF TABLES

Chapter 1

INTRODUCTION

1.1 INTRODUCTION

Nanoimprint lithography (NIL) is an integrated circuit (IC) patterning system, which is competing with other techniques to become the next generation lithography technique (NGL). NIL is a very simple patterning system that uses a mold, which is pressed into a deformable resist to replicate patterns. This allows it to reproduce incredibly fine features using relatively inexpensive equipment.

Current deep ultra-violet (DUV) lithography techniques have a finite resolution limit which the industry will soon be approaching. To continue to fabricate smaller and smaller features, a NGL technique is required. The choice of technique will be determined by how each system performs. Resolution, reliability, throughput and cost are some of the factors that the industry will use to make this decision.

NIL also has a high potential for a niche area that no other current lithography technique can provide for, and that is for multilevel fabrication. Due to the stamping nature of imprint, the only specific requirement to produce 3D structures is a multilevel stamp [1]. This could allow for huge simplification for producing on-chip micro optics, micro-electrical-mechanical devices, biochips and T-gate transistors [2].

1.2 NANOIMPRINT LITHOGRAPHY

Nanoimprint lithography has been identified as one of the major competing lithography methods to become the next generation lithography (NGL) technique. Most NIL concerns have been addressed [3], and commercial imprint steppers capable of sub-50 nm resolution with sub-10 nm 3σ alignment are available [4]. The other main contenders include extreme ultra-violet (EUV), X-ray lithography and parallel maskless photo lithography.

Basic imprinting techniques were first formed around 3500 BC when the Sumerians developed cylinder seals which were rolled into soft clay to reproduce the pattern. It also has similarities with inking methods and manufacture of CD and DVDs. NIL is

a simple and reliable technique where the process is not the limiting factor for future resolutions, as sub 10 nm features [5] and even 14 nm periods have been achieved [6].

The use of imprint lithography in micro and nano lithography was first envisioned by Richard P. Feynman in his talk at the annual meeting of the American Physical Society at Caltech on the 29th of December 1959, entitled: 'There is Plenty of Room at the Bottom'. It was not referred to as Nanoimprint Lithography, but the technique described is very similar to the first NIL performed [7]. Since his talk only relatively little progress had occurred until recently. The advent of Compact Disks (CDs) in the 1980's were the first mass usage of imprinting for producing micro scale features. However imprint technologies was not further investigated until Stephen Chou et al, started performing true nanoimprint which was reported in 1996 [7]. Since then a steadily increasing number of researchers have investigated NIL and related techniques improving resolution, imprinting area, overlay accuracy, uniformity and a number of other important requirements.

1.3 MOTIVATION

Maintaining the current microelectronic miniaturisation trend, which follows Moores law [8] - doubling the number of transistors per integrated circuit every two years, lithography techniques are being forced to produce smaller and smaller features. The current mainstream process are based on either 193 or 157 nm DUV excimer laser light sources to produce minimum sized features between 130 to 50 nm. From these wavelengths and shorter, it becomes difficult to find suitable materials from which to produce lenses, as the current materials, calcium fluoride (CaF_2) and barium fluoride (BaF_2), become increasingly birefringent at certain crystal orientations [9, 10]. A solution around this problem has been adopted for extreme ultra violet (EUV) lithography by using exclusively reflective optics. However while EUV has a potential resolving size of 15 nm, it is inefficient, requiring large amounts of electricity and very expensive optics.

So alternative technologies have, and are now, being investigated for sub 100 nm lithography. Amongst these are nanoimprint and its variants, electron beam, local oxidation, X-ray, maskless DUV [11], EUV and focussed ion beam (FIB) lithography. Three of these techniques (EBL, FIB and local oxidation) are severely bottled-necked by the serial process in which the pattern is written, however they are suitable for very high resolution patterning. FIB lithography is better suited for 3D lithography as it either builds or etches structures very controllably. Maskless DUV lithography overcomes a number of issues of DUV lithography, including mask cost (a major cost for modern devices), and feature (corner) compensation since light coherence has no bearing on exposure levels. This technique is still limited by the diffraction limit, if not to the extent current DUV technology is. EUV has a number of complex and costly

problems to resolve before becoming viable, including throughput, power consumption, lens reflectivity, and the need for ultra clean environments [12, 10]. X-ray lithography is difficult as X-rays cannot be reflected or refracted, making focusing and collimating difficult. Also due to their high energy X-rays are very difficult to block and require very thick masking materials.

As the technology produces smaller and smaller devices, the cost of ownership (CoO) increases exponentially. Current DUV lithography tools cost around $15 million US each [13], with $50-75 million expected to be hit for EUV tools. With NIL on the other hand, there is no foreseeable huge cost involved with increasing the resolution, apart from mask and alignment costs. Coupling this with the fact that NIL can perform 3D fabrication in a simple and quick step, makes it economically competitive with capabilities unavailable to other techniques.

1.4 THESIS OBJECTIVES

It is the aim of this study to fabricate in a single lithography step high resolution structures that feature variable structure height for use as a mold in nanoimprint lithography. By performing this in a single lithographic step, costly and time consuming alignment steps can be avoided allowing for cheaper, simpler and faster processing. The areas of attention include the resist coating, pattern exposure, dry etching and anti-sticking layers. Once developed, the mold will be imprinted into a polymer.

1.5 THESIS OUTLINE

Figure 1.4 shows the flow for the mold development and imprinting techniques used in this study. This thesis has been separated into six chapters, organised as follows.

Chapter 2, background, covers existing imprint techniques, including nanoimprint lithography, reversal imprinting, wafer scale imprinting, step and stamp, step and flash imprint lithography and three-dimensional imprint lithography, along with the advantages and disadvantages of each.

Chapter 3, experimental techniques, covers the experimental techniques, and some of the basic theory behind them, used in this study to fabricate the NIL molds. This includes sample preparation, resist coating, soft baking, electron beam exposure, development, metallisation and reactive ion etching. Inspection methods, including atomic force microscopy, optical microscopy and scanning electron microscopy are also covered.

Chapter 4, mold fabrication, goes into detail about the actual mold fabrication work performed including results of successful and unsuccessful fabrication procedures. This includes resist processing, pattern exposure, metallisation and etching procedures.

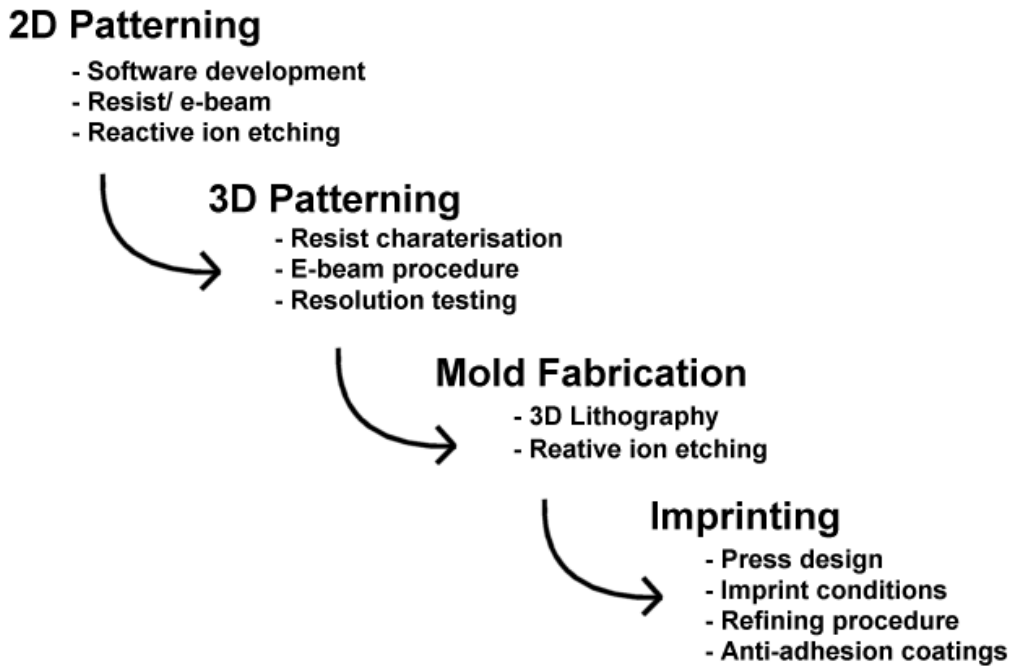

Figure 1.1 Overview of the research that forms the basis of this thesis. The work can be broadly divided into two main stages. The first is mold fabrication, which consisted of developing and fine tuning the fabrication procedures as well as the actual mold fabrication. The second stage is the imprint of the molds into a thermal plastic, and related topics.

Chapter 5, imprinting, discusses the results of imprinting experiments characterising the effects pressure, and heating have on the imprint out come. Resist sticking issues are also visited.

Chapter 6, conclusions and future work, discuss the results obtained from experiments, outlines the best techniques found, and describes how these results can benefit the real world. There is also a discussion on areas in relation to 3D NIL that could, in the authors opinion, benefit from further research.

Chapter 2

BACKGROUND

2.1 OUTLINE

This chapter is concerned with a overview of several imprint techniques that are in use today, how they work and advantages and disadvantages of each. Further information is also provided on anti-stick coatings, and the uses and limitations of imprint lithography.

2.2 IMPRINTING TECHNIQUES

Since it was first published in 1996 [7], imprinting techniques have been developing as researchers have been finding methods to overcome current problems and find solutions to getting imprint to work for new applications. NIL was the first technique to be discovered, however variations quickly followed suit in the few years after 1996. Some of these techniques are described in this section.

2.2.1 Nanoimprint Lithography

Nanoimprint lithography is the first of numerous imprint techniques today to be explored. Also known as hot embossing lithography, the mold is pressed into a thermal plastic layer which has been heated above its glass transition temperature, which deforms taking the molds shape. The basic steps are illustrated in Figure 2.1.

The first step of imprinting, as with most lithography techniques, is to prepare the target sample. This is done by first cleaning, then applying the imaging layer. For NIL a thermal plastic is generally used. The patterned mold, consisting of high and low regions, is then placed face down on the target sample and he two are heated and pressed together. The temperature applied is generally between the glass transition temperature (T_G) and decomposition temperature (T_D) of the polymer. They are held like this for a set period of time to allow the polymer to flow away from the high regions of the mold into the low. They are then cooled and separated. After separation there is always a small residual layer, illustrated in Figure 2.1(d), where there should ideally be none. This can be removed by a very quick dry etch, called a break through etch.

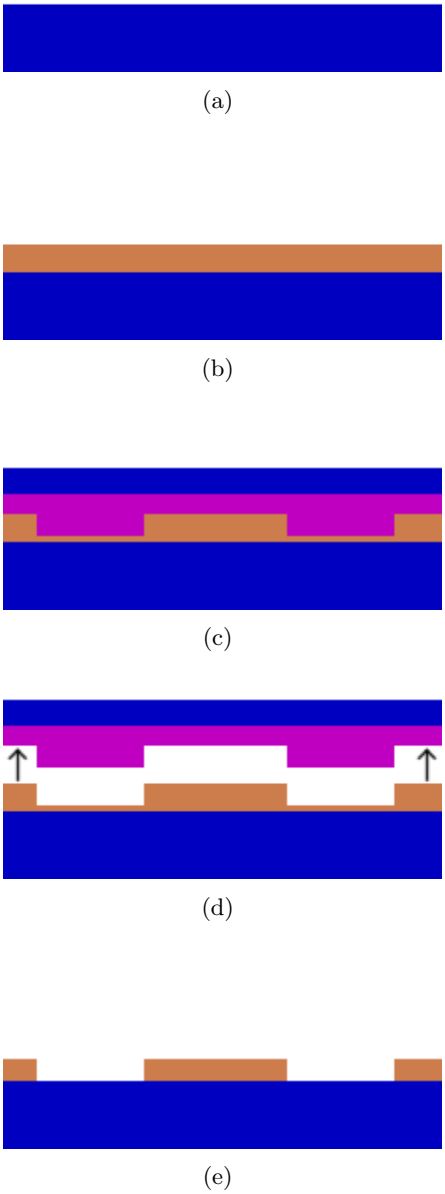

Figure 2.1 The basic steps of nanoimprint lithography. First clean the sample (a), coat with a deformable thermal plastic (b), place mold face down on sample and heat and press (c), cool and release after a set time (d), and perform a breakthrough dry etch (e).

The mold can be made from almost any material, depending on the manner in which it will be used. Nickel molds have been used extensively [14, 15], but other materials such as Si [16], SiN [17, 1], SiC and diamond [5], PDMS [18, 19, 20], quartz [21] and fused silica [16] have also been investigated. Some, like SiC, SiN and diamond, are particularly well suited to NIL as they are very strong materials which do not deform or damage easily. SiC and diamond have even been used directly to imprint into metal [5]. Others such as diamond, quartz and fused silica can be used for UV curable techniques as they are transparent materials.

The thermal plastic includes a very wide range of materials. They are generally polymers which are spin coated onto the sample and have a T_G that is lower than their T_D. PMMA is once such polymer and has a T_G around 105 °C and a T_D of 375 °C, and imprint temperature is often around 160 °C [22]. Other materials can be substituted for the thermal plastic, such as a thermal or UV curable monomer, and form the basis of some of the other imprint techniques.

The residual layer can also cause problems. If the mold has features of varying sizes, the residual layer can vary in thickness as a result of the polymer flow. This is because larger structures need to displace larger amounts of polymer across greater distances than small structures. This tends to mean the residual layer is thicker under large structures, with the tallest part in the centre. If the difference is large enough it becomes difficult to find a critical etch time that removes all the residual layer, but none of the valid structures, as illustrated by Figure 2.2.

Due to its simplicity, NIL has an advantage that it can be used to pattern whole wafers at a very high resolution in a single step. This is unlike commercial DUV technology which would be prohibitively expensive to manufacture such a tool. Imprint of 4" and 6" wafers has been reported [23, 16] with a minimal residual layer, and an in-depth study has been performed into producing reliable 8" wafer imprints [24].

Heating the mold and sample combination can also cause severe alignment problems. This is caused by the difference in materials and uneven heating and or cooling of the mold and sample. For instance the thermal expansion coefficient of a quartz mold is $7.4\times10^{-6}\mathrm{K}^{-1}$, and if used in conjunction with a silicon wafer ($2.6\times10^{-6}\mathrm{K}^{-1}$) there is a difference of $4.8\times10^{-6}\mathrm{K}^{-1}$. This means an expansion difference of 480 nm over a 4" wafer for increase in temperature of both mold and wafer by 1 K. Even if the temperature is held very steady with only 0.1 K deviation from the ideal temperature, a 48 nm difference would have severe effects on alignment with sub 100 nm patterns. Ideally both the mold and sample being imprinted need to have been produced from materials with very similar expansion coefficients and only small areas being patterned. For instance, fused silica ($0.54\times10^{-6}\mathrm{K}^{-1}$) and silicon have a thermal expansion coefficient difference of $2.06\times10^{-6}\mathrm{K}^{-1}$, meaning for a 10 mm square area with 0.1 K temperature the variation from ideal has a misalignment of 2.06 nm, which is acceptable. So

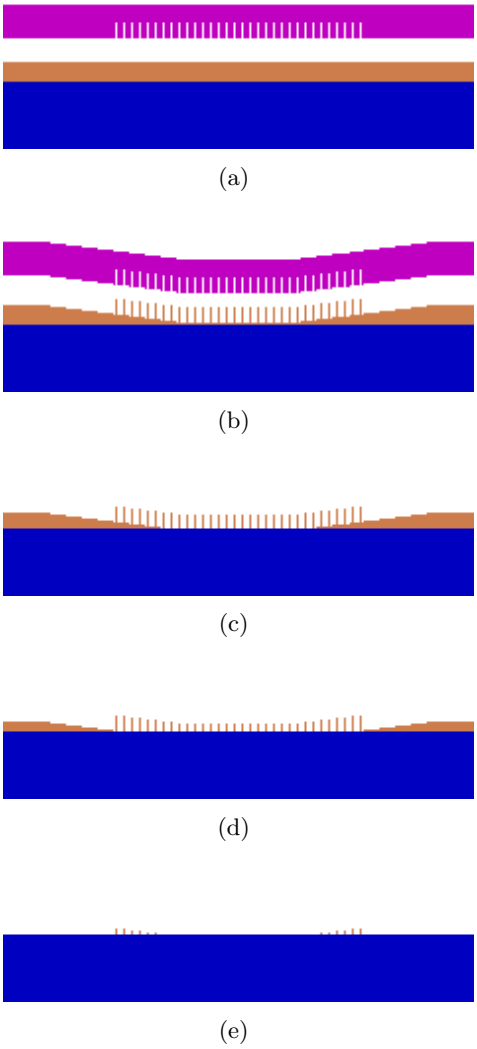

Figure 2.2 The problem that occurs if overly large structures are imprinted. Due to their size, the large raised areas to either side of the pillars on the mold (a) cause the mold to bow during imprinting and do not imprint deeply into the resist (b). This causes problems for the break-through etch. If a minimal etch is performed, not all the pillars are etched through to the substrate (c). If it is etched so that all the pillars are separated on the substrate (d), the large areas either side are still covered. If the etch is allowed to continue far enough, they are removed, but so are the middle pillars (e).

to prevent thermal problems, only small areas should be patterned at a time and the mold and target materials should have a similar thermal expansion coefficient with both being held very close to an ideal temperature. This rules out using both thermal plastic or thermal curable polymers for achieving high alignment accuracy.

2.2.2 Reversal Imprinting

Reversal imprinting, also called inking, is an interesting variation of standard imprint lithography. Instead of coating the resist onto the target sample, it is coated onto the mold [25]. This is then pressed on target, and only the resist in contact with the target is transferred. This process is shown in Figure 2.3. The main limitation to the pattern transfer is that the resist should adhere better to the target structures than the mold. Since only the raised structures on the mold are transferred, the target need not be a flat area, and in fact can be performed on an already patterned surface. This can allow quick and simple construction of photonic lattices [26].

2.2.3 Step and Stamp

While it is possible to parallel pattern large areas such as wafers, thermal problems as mentioned in Section 2.2.1 make it impractical. The other option is then to do the current industry norm of patterning a small area and stepping to the next location before repeating. This means that the master only needs to be a single copy of a pattern rather than a wafer size master, making it simpler to produce. Since the pattern is smaller, the total thermal expansion is also smaller meaning less overlay problems.

2.2.4 Step and Flash Imprint Lithography

While step and stamp relies on imprinting into a thermal plastic or curable monomer, step and flash imprint lithography (SFIL) imprints into a UV curable monomer, such as hydrogen silsesquioxane (HSQ) [27, 28] or spin on glass (SOG) [29], as illustrated by Figure 2.4. There are a number of useful advantages to this method. Firstly, since a transparent mold must be used, optical alignment is possible so that markers on the mold can be overlaid with markers on the target sample. Secondly, since the monomer is UV curable it is still liquid when the mold is placed face down, meaning very little pressure is required to press the mold into it, and it allows for some lubrication so that mold can be moved laterally for alignment. Since the monomer layer can be applied via either spin coating or a number of tiny drops, it is possible to adjust the amount from area to area to account for changes in pattern density. SFIL operates at room temperature with only minor heating from the UV light, preventing thermal problems. It has also been shown that masks are self cleaning throughout the imprinting process

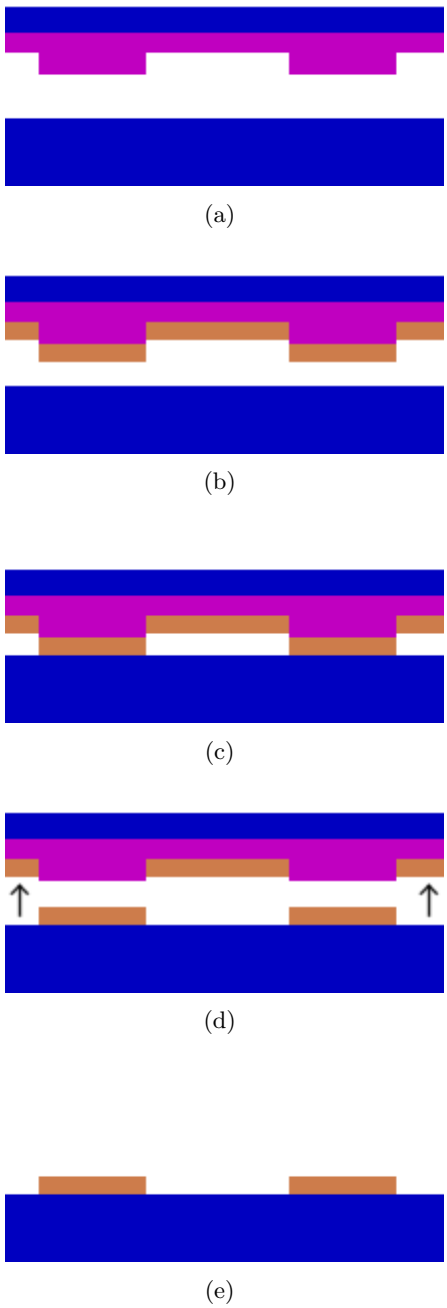

Figure 2.3 Reverse imprint lithography. First clean both mold and sample (a), coat mold with resist (b), place mold face down on sample and press (c), then release (d), producing the final pattern (e).

[30] so after a number of imprints, all contaminants have been removed from the master. A recent study has shown that a near zero residual can be reliably obtained [31].

2.2.5 Anti-sticking Layers

During the imprint process the mold and the resist layer come into intimate contact. If the adhesion between the resist and mold is greater or similar than that between the resist and substrate, part or all of the resist will remain stuck to the mold after separation. To prevent such issues, ideally the mold will be coated in a durable, thin, very low adhesion coating which is unaffected by most cleaning agents. If the coating is too thick, the thickness of features on the mold can become compromised leading to undesirable results, and likewise if the durability is insufficient or it is not resistant to cleaning agents, the coating would need to be reapplied regularly. Currently one of the more popular anti-stick agents in use is a self assembled monolayer (SAM) consisting of trichloro(1H,1H,2H,2H-perflouroоctyl)silane [32, 33], also known as FOTS or $CF_3(CF_2)_5(CH_2)_2SiCl_3$. It can be easily applied via either vapour or liquid phase exposure and, with the presence of surface water, reacts and covalently bonds to the surface. This is illustrated in Figure 2.5.

FOTS has a very low surface energy, and since it covalently bonds to the substrate surface, it is a very durable coating which is resistant to both acids and bases. Prior to coating, the samples are placed in a humidity chamber to ensure a water film covers the entire surface, however droplets should not be visible. To coat a sample by vapour phase, it is then placed in a sealed box along with a small amount of FOTS in a beaker. Some of the FOTS evaporates out of the beaker and becomes deposited on the sample. After a set period of time, the sample is removed and is annealed between 100 and 150 °C for a period of 15 to 30 minutes. Liquid phase deposition occurs by then mixing the FOTS in with a solvent and and dipping the samples into for a set period of time, ranging from 1 to 30 minutes. These are then annealed in a similar fashion to the vapour phase exposure.

2.3 THREE-DIMENSIONAL NIL

By its very nature, NIL is a three dimensional lithography technique, even though most of its use has been focused towards two dimensional fabrication. In fact NIL is the only lithography technique available today which can quickly and accurately produce 3D structures. Other techniques which can produce 3D structures, but not as quickly and easily, are multiple step photo, e-beam or X-ray lithography. FIB and EBL can be used to directly create 3D structures, however due to the serial nature of the writing, it is a very slow process. Nil has an added difficulty when producing 3D structures is that any bowing of the mold will affect the height accuracy of features.

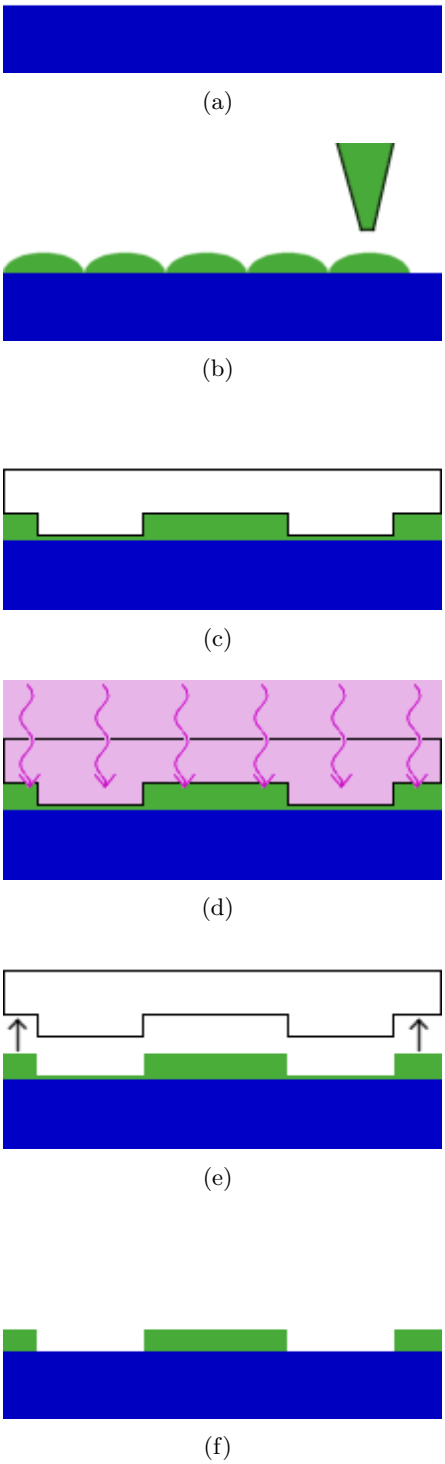

Figure 2.4 Step and flash imprint lithography. First clean the target sample (a), then deposit UV curable monomer (b), place mold face down on sample and align via optical marks (c), expose monomer to UV light (d), remove mold (e), then repeat steps (b) through (e) for subsequent imprints on the same wafer, and finally carry out a residual layer dry etch (f).

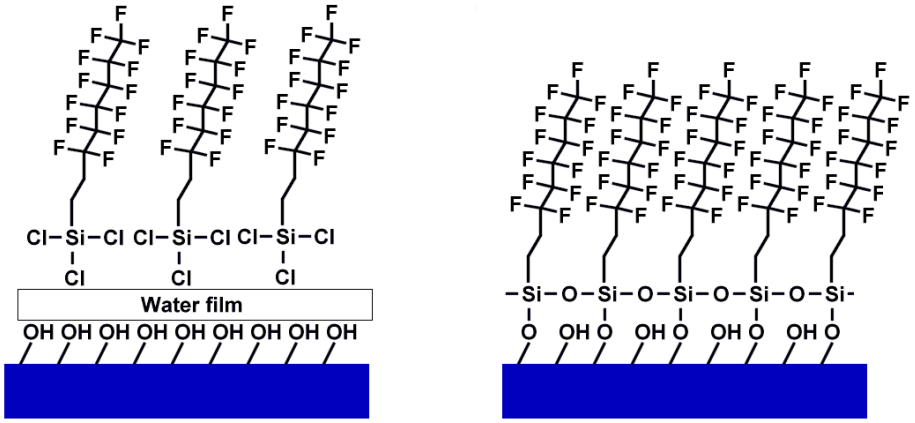

(a) (b)

Figure 2.5 How trichloro(1H,1H,2H,2H-perflourooctyl)silane covalently bonds to a silicon substrate. (a) the sample is exposed to the FOTS chains either through liquid or vapour phase while there is a water film present on the surface. (b) The sample is then annealed so that the chlorosilane reacts with the surface water allowing for a Si-O-Si covalent bond to the surface.

2.4 USES OF NIL

The highest resolution believed to be produced by EBL to date has been a 23 nm period [34], which is larger than the 14 nm period achieved by NIL [6]. This indicates that NIL can perform extremely high resolution imprint, limited mainly by the technique used to produce the molds. The uses of NIL and its variants are far ranging - not only is it useful in the integrated circuit industry, but for chemical applications by allowing for very simple and direct inking of patterns without the need for exposure, development and further processing on expensive tools. A combination of the imprint techniques can be used to manufacture complex multi-layer devices [35].

Three-dimensional NIL will have high potential for producing multilayer structures including the simplified fabrication of MEMs devices, on chip optics, T-gate transistors, biochip, and room temperature single electron transistor (SET) [36] applications.

2.5 LIMITATIONS OF NIL

While NIL appears to be an incredibly useful tool across a large range of areas, it does come with some disadvantages. Firstly, the mold needs to be fabricated by some other method (usually EBL) at a 1:1 scale, which for high resolution patterns means a very long and expensive write. DUV does not have this problem as commercial mask steppers often use a 4:1 reduction ratio, meaning that the larger features on the mask can be produced more quickly. Similar to DUV lithography, it is a costly exercise to alter patterns, due to the time and tools required to replace all the masks. Since NIL is a contact lithographic method, the masks will inevitably become damaged, causing

ongoing costs to replace or repair them.

2.6 SUMMARY

This section has described several imprinting techniques and the advantages and disadvantages of each. It would seem that NIL and its related techniques have a bright future ahead of them. They are capable of very high resolution patterning for relatively low cost when compared to DUV, X-ray, EUV or e-beam lithographic techniques. Each technique will find its own use, and it seems that SFIL will become the most important for producing ICs.

Chapter 3

MICROFABRICATION TECHNIQUES

3.1 OUTLINE

This chapter covers the basic theory and most of the processes and procedures required to produce NIL molds described in this study. These include the cleaning, resist coating, EBL patterning, development, lift-off and dry etching. At the end, inspection techniques are covered as well as the basics of how they perform.

3.2 SAMPLE PREPARATION

Samples, 10 mm^2 square, were diced from 4" silicon wafers coated with a 1 μm thick low stress silicon nitride (Si_xN_y) layer deposited by low pressure chemical vapour deposition (LPCVD).

A protective coating of $\sim$ 1 μm thick photoresist was spin coated onto the wafer prior to scribing to prevent Si and Si_xN_y dust from becoming embedded in the surface. The scribing tool (shown in Figure 3.1) was built by the University of Canterbury (UoC). The wafer was aligned by placing the flat edge against the alignment pegs on the holder which was in turned placed on the stage and could be rotated by increments of 90 °. A vacuum was then applied to hold both the wafer and holder in place on the stage. The stage could move freely back and forth, and the diamond stylus could be accurately moved across by the worm gear with positions marked every 10 μm. Once in place the stylus was lowered and the stage pulled forward to scribe a single clean line. The wafer was scribed every 10 mm on the back surface as the Si_xN_y layer crystal structure was not aligned to the Si substrate, and so does not cleave as well. To scribe perpendicular lines, the holder was rotated by 90 ° and the process repeated. The wafer was cleaved by gently exerting even pressure across the surface while the scribe line was aligned over a straight edge.

The samples were then cleaned by the ultrasonic bath shown in Figure 3.2 with immersion in acetone, then methanol and finally isopropyl alcohol (IPA) for 5 minutes each. After being cleaned with each solvent the samples were blown dry using a nitrogen

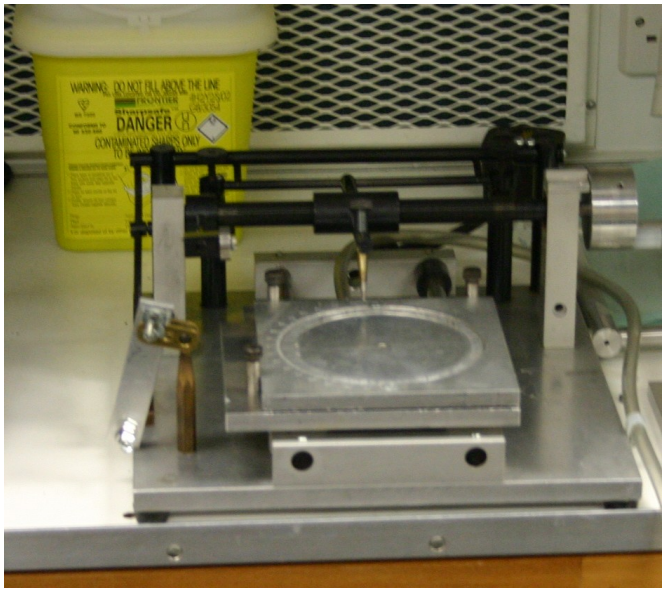

Figure 3.1 UoC built wafer scriber. The stage can move forwards and backwards, while the diamond tip stylus can be accurately positioned by use of the dial on the right.

Figure 3.2 Ultrasonic bath and recirculating fume hood at UoC.

gun. The samples were then placed in a covered glass petrie dish and stored at 185 °C to evaporate and maintain a water free surface.

3.3 RESIST COATING

In almost all cases pattern transfer requires a resist layer to pattern, whether it is photo, electron or imprint lithography. Spin coating is a simple and easily repeatable process, controllable by altering the spinning speed, acceleration, deceleration and spinning time. A basic schematic can be seen in Figure 3.3. More complicated spinning processes may involve several stages at various different speeds and possibly with a controlled atmosphere.

The resist thickness can be calculated from Equation (3.1) [37] where h_0 is the initial resist thickness (m), f the rotational speed (r/s), η the resist viscosity (m^2s^{-1})

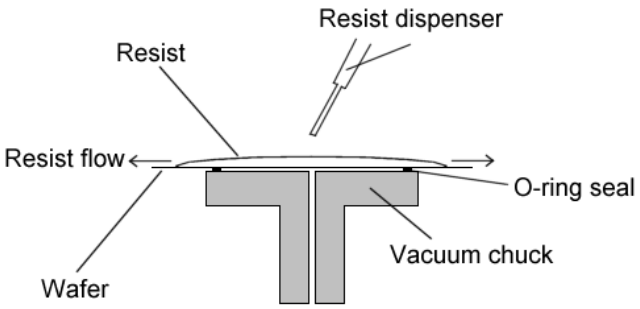

Figure 3.3 Resist spinning process. The wafer is held in place by a vacuum applied to the chuck and sealed with an O-ring. The resist is deposited in the centre of the wafer, which is then spun at several thousand rpm. This causes the resist flow outwards, producing a smooth uniform layer.

and t is the spinning time (s).

$$h = \frac{h_0}{\sqrt{1 + \frac{16\pi^2 f^2}{3\eta} h_0^2 t}} \tag{3.1}$$

As t increases the addition of 1 becomes insignificant, and when removed allows cancellation of the h_0 term, generating Equation (3.2).

$$h = \frac{\sqrt{\frac{3\eta}{t}}}{4\pi f} \tag{3.2}$$

Here we can see that the resist thickness depends mainly on the spinning speed, time and fluid viscosity, but only on the condition that t is significant enough. This, however, does not account for the resist edge bead, where surface tension holds some excess resist around the edge of the sample. This usually affects the resist within 1 - 2 mm of the edge, however it has a larger effect on square samples than round wafers. It can be removed by solvent, but it was not deemed necessary for this study, and care was taken not to use the areas of the samples affected by it.

A Laurell Technologies WS-400B-6NPP/LITE [38] spinner was used, pictured in Figure 3.4. It consisted of a vacuum chuck to hold samples, had a splash cover with a hole for applying resist onto the sample and allowed for several process stages. The parameters used throughout this study were 4000 RPM, a spin time of 60 s, an acceleration time of 5 s and the fastest deceleration possible.

The samples were removed from the drying oven and allowed to cool to room temperature before spin coating commenced. Each sample in turn was placed in the centre of the spinning chuck and then the vacuum was applied, holding the sample firmly in place. A quick blow from the nitrogen gun removed any small debris which

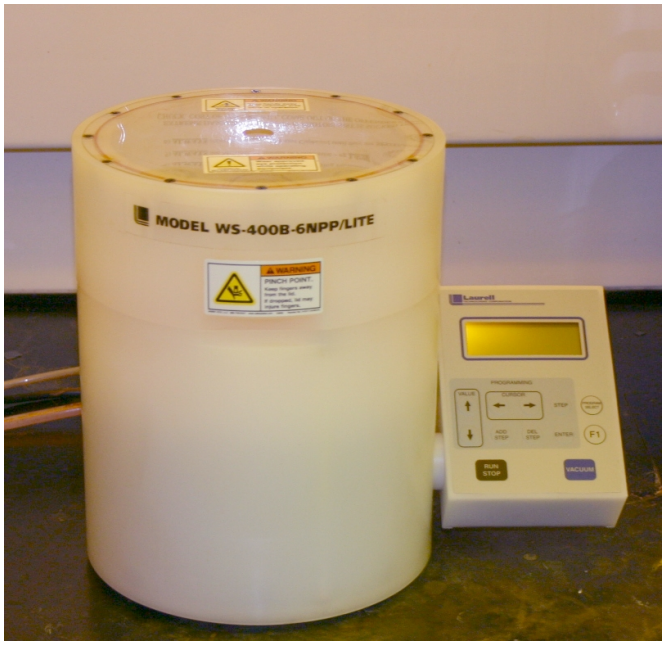

Figure 3.4 Laurell technologies spinner in the UoC laboratory.

may have accumulated on the surface, and the splash cover closed. The required number of drops of resist were then deposited into the centre of the sample via a 1 mL disposable pipette through the hole in the splash cover and then the spinner was immediately started. The amount of resist applied was around 60 μL, far exceeding the 20 nL volume in a 200 nm thick layer. However the large amount was necessary to ensure that mass of the resist could overcome the surface tension, allowing the whole sample to be evenly coated. The excess resist is flung off during spinning. This is due to the surface tension being insufficient to overcome the centrifugal forces.

To aid the removal of any solvent remaining in the spun resist, the sample was heated prior to exposure. This is called soft baking or the pre-exposure bake. There are a number of ways of doing this, from a hotplate bake, infra-red (IR), microwave heating or convection oven.

3.3.1 Spin Coating PMMA

Poly(methyl methacrylate) (PMMA) is a very stable positive e-beam resist, with a shelf life of several years. The molecular structure can be seen in Figure 3.5. PMMA is used for two different applications in this study. The first is for electron beam lithography which required a two layer resist stack, and the other use is for imprint lithography which only requires a single layer to imprint into.

The two layer resist stack is used to create a good profile for performing lift-off. This works because the bottom layer develops more readily then the top layer resulting in an undercut profile. The bottom layer was spin coated first using 2 drops (around 60

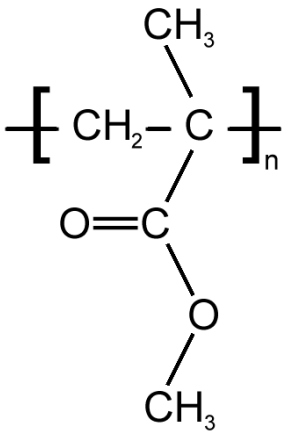

Figure 3.5 Chemical structure of PMMA. The higher the molecular weight, the higher n is. For a molecular weight of 30 kg/mol, n is around 360, and for 120 kg/mol, n is near 1,430. When it is exposed, the chains break up into smaller, more soluble sections.

μL) low molecular weight (LMW, M_g = 30 kg/mol) PMMA. This layer was pre-baked at 185 °C for 30 minutes in a Sanyo Drying Oven MUV112. The LMW PMMA was thinned to 4% by weight in xylene and resulted in 120 nm thickness. A second layer, consisting of 2 drops of high molecular weight (HMW, M_g = 120 kg/mol) PMMA, was then spin coated. Again the sample was pre-baked at 185 °C for 30 minutes. The HMW PMMA was thinned to 2.5% by weight in xylene giving a resist thicknes of 80 nm, and the overal resist stack a thickness of 200 nm.

The PMMA layer used in imprinting was a single coating of LMW PMMA, around 120 nm thick. LMW was used as it has a smaller polymer chain length than the HMW, so having a slightly lower T_g (glass transition temperature), and can be deformed more readily at lower temperatures [39].

3.3.2 Spin Coating ma-N2403

For producing 3D molds, Microresist's ma-N2403 negative tone DUV and e-beam sensitive resist was used [40]. This resist, when developed, has a thickness almost linearly proportional to the exposure dose. This fact and its high selectivity when used in dry etching make it ideal for fabricating 3D structures.

It was necessary to use a primer with the resist, as small structures would often detach from the surface during development. This involved spin coating one drop of hexamethyldisilazane (HMDS) primer onto the surface immediately prior to spin coating 2 drops of the ma-N2403 resist. The HMDS increases resist adhesion to the substrate by chemically bonding the to surface via a reaction with water and providing a large number of 'branches' for the resist to attach to. The chemistry of this is shown in Equation (3.3), and illustrated in Figure 3.6.

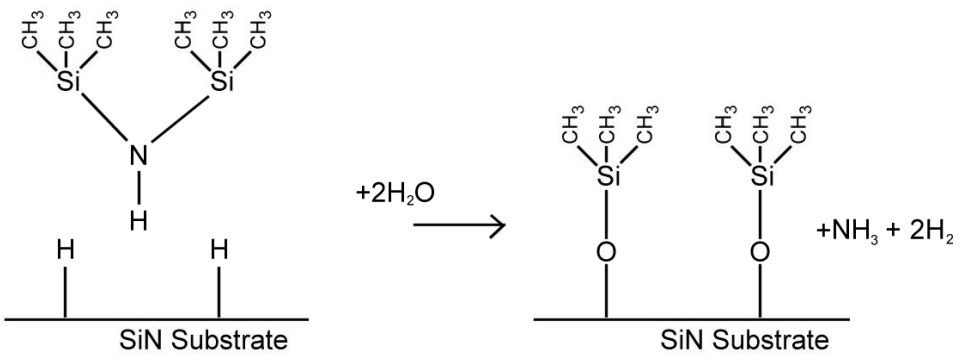

Figure 3.6 HMDS chemical structure. The nitrogen reacts with water creating NH_3 and H_2, while oxygen attaches to the $Si(CH_3)_3$ parts and covalently bonds to the substrate surface, leaving the methyl groups providing ample sites for the resist to attach to.

$$2Si_xN_y : H + HN(Si(CH_3)_3)_2 + 2H_2O \longrightarrow 2Si_xN_y : OSi(CH_3)_3 + NH_3 + 2H_2 \quad (3.3)$$

The resist thickness was always measured after the pre-exposure bake. After soft baking the resist thickness was 300 nm. When the resist had been thinned by Microresist's ma-T1024 thinner by equal volumes the soft bake thickness dropped to 75 nm.

3.4 ELECTRON BEAM LITHOGRAPHY

Electron beam lithography (EBL) is an extremely powerful tool for creating patterns and remains the primary method for producing high resolution photo lithography mask reticles. EBL allows for very high resolutions due to the short electron wavelength, given by Equation (3.4) discovered by de Broglie [41]. h represents Planks constant (6.626×10^{-34} J s), m the mass of an electron (9.11×10^{-31} kg), v the velocity of the electron (m/s), while λ is the resulting wavelength (m).

$$\lambda = \frac{h}{mv} \quad (3.4)$$

$$Resolution(W) = \frac{k\lambda}{NA} \quad (3.5)$$

This links the wavelength of a body to its momentum, so as the bodies velocity increases, its wavelength decreases. Equation (3.5) shows the correlation between the electron wavelength and the diffraction resolution limit. k is the Rayleigh constant, which describes the difficulty of resolving features, NA is the numerical aperture of the imaging system, with 1 being a very good value and 0.1 being poor, while W is the maximum resolution obtainable (m). This means that an electron with a kinetic

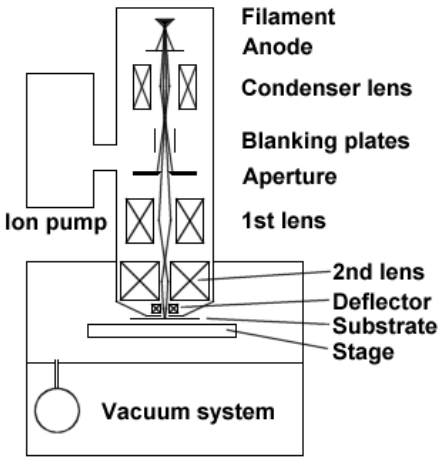

Figure 3.7 Diagram of the workings of a EBL system. The electrons are emitted from the tip (a) and are accelerated by the voltage potential between the anode (b) and cathode (c), passed through a aperture (d) to shape the beam and limit the current. From here the beam is condensed and focused (e,f) and x-y deflected (g) before the final focusing stage (h) and arriving at the sample surface.

energy of 10 keV has a wavelength around 3.9×10^{-4} nm, and when combined with the diffraction limit equation (with poor values for both k and NA) still gives a resolution limit around 1×10^{-3} nm. This is substantially smaller than the lattice spacing of silicon (5.43×10^{-1} nm), showing that the electron wavelength is not the limiting factor of e-beam lithography. While electrons allow for very high resolutions, the beam diameter and resist used limit the resolution potential. The serial writing of patterns means that it is a low throughput technique, limiting its viability for direct production lithography, however it is economical enough to create masks and molds which can in turn be used for mass production.

Electron beam lithography works by focussing a beam of electrons emitted from a fine tip into either a point a few nanometres in diameter or particular shape on the target substrate. Figure 3.7 shows a basic parts of a EBL system. By scanning this beam in both x and y directions by either magnetic or electrostatic deflection, and blanking the beam on and off, one can write a pattern into a electron sensitive resist. Since electrons are readily absorbed by almost any medium, including air, the electron beam and samples must be in placed in an high vacuum chamber.

Figure 3.8 shows that from the resist surface downwards, the electrons' path can be deflected allowing some electrons to be reflected off the surface (secondary electrons), and others to deflected internally, giving rise to lateral movement. The distance an electron travels in the substrate is mainly determined by its kinetic energy. By increasing the acceleration voltage, the electrons will penetrate further into the substrate, and while the initial scattering angle (forward scattering) decreases, the overall scattering distance increases. Reducing the resist thickness is a method of reducing forward scattering, allowing for higher resolution structures.

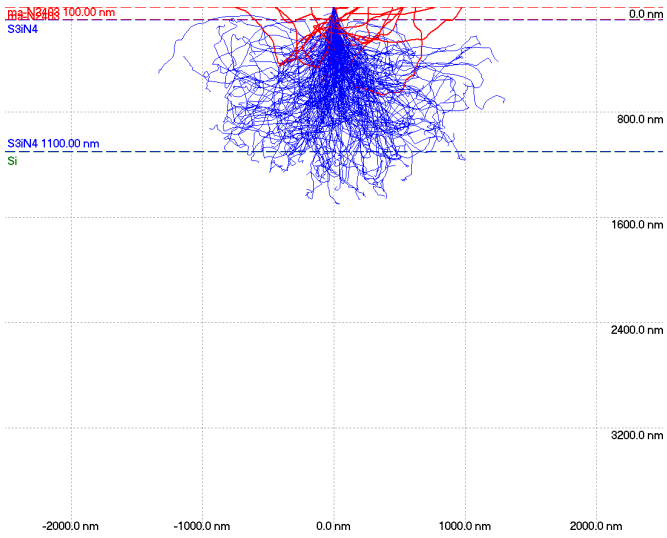

(a)

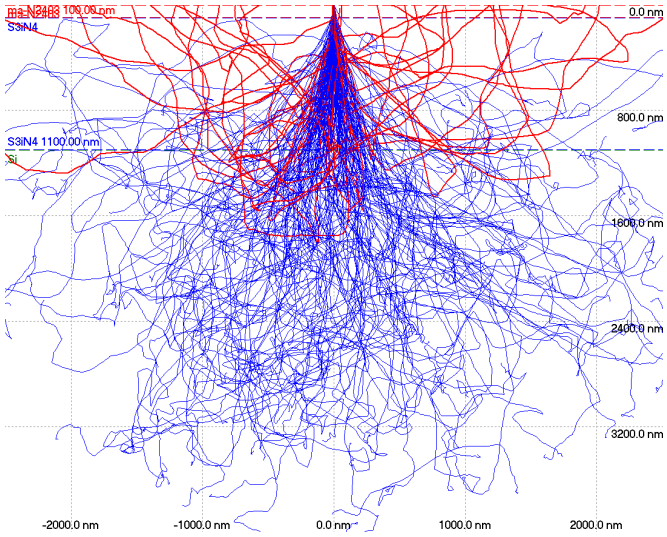

(b)

Figure 3.8 A Monte Carlo simulation of the scattering path of 200 electrons in the resist/substrate stack. Blue lines are the electron which come to rest in the sample, while the red lines are the backscattered electrons and give rise to the proximity effect. (a) Shows the paths by electrons with an energy of 10 keV, while (b) shows the paths for 20 keV.

By correlating the number of secondary (reflected) electrons and the location of the beam, one is able to build up an image of the surface. This is the method by which scanning electron microscopes (SEM) work. This is discussed in further detail in Section 3.11.3.

There are a number of fundamental complications to operating EBL tools, which can be compensated for if due care is taken. Electrons, unlike photons, are charged particles and repel one another. This is only a small effect which only becomes pronounced in very high current density or low acceleration tools, and can normally be ignored. Other factors, such as proximity exposure cannot be ignored all the time and must be compensated for. This is where the region around the target exposure area becomes slightly exposed, causing potential bridges between adjacently exposed areas. This can be countered by slightly decreasing the exposure dosage near dense patterns so that the dosage to the unexposed area stays below the critical dosage. Some systems have software which can automatically account for this phenomenon and compensate for it.

Due to the required pixel spacing and the e-beam deflection limitations, the largest area that can exposed at a time is often limited to a few thousand μm^2. To expose larger areas, it is broken up into smaller write fields and exposed sequentially. The write fields need to be accurately measured out and aligned to each other to provide a continuous pattern. This means that the write field size, shape, rotation and position all have to be very accurately specified.

3.4.1 Philips PSEM500

The initial work performed in this study was done on a Philips scanning electron microscope (PSEM500) shown in Figure 3.9 and had been converted by UoC for lithography use. This system used a tungsten filament along with a stepper motor driven stage. The stage movement had play in the order of several microns. The alignment of adjacent write fields or consecutive exposures on the same area were rarely acceptable. The beam scanning was performed by a UoC built control system, and with careful work, resolutions down to 70 nm could be obtained. Various magnifications could be used to adjust the write field size from 7,030 $\times$ 4,495 μm down to 1.72 $\times$ 1.23 μm. The beam could be addressed to any place inside the field by two 12-bit digital to analogue converters (DACs), with one of each controlling the x and y coordinates. Table 3.1 gives the available write field size and the minimum possible pixel spacing.

L-EDIT is used to generate patterns for the PSEM500, which are then exported as CIF (Caltech Intermediate Format) files, which is then converted by UoC developed program into a format usable by the PSEM500 pattern generator. These are then transferred to the EBL by floppy disk and written from there.

Figure 3.9 UoC Philips PSEM 500. The UoC built pattern generator is located to the left.

Table 3.1 Available write fields and minimum pixel spacing for the PSEM500

Magnification	Write field size (μm)		Pixel Spacing (nm)	
	X	Y	X	Y
20	7,030.00	4,495.00	1716.0	1,097.0
40	3,513.00	2,248.00	858.1	548.7
80	1,646.00	1,097.00	401.7	267.8
160	868.70	604.00	212.1	147.5
320	434.60	296.30	106.1	72.3
640	222.20	153.10	54.3	37.4
1,250	114.20	76.47	27.9	18.7
2,500	57.84	38.73	14.1	9.5
5,000	28.43	18.63	6.9	4.5
10,000	14.22	9.80	3.5	2.4
20,000	6.86	4.90	1.7	1.2
40,000	3.42	2.45	0.8	0.6
80,000	1.72	1.23	0.4	0.3

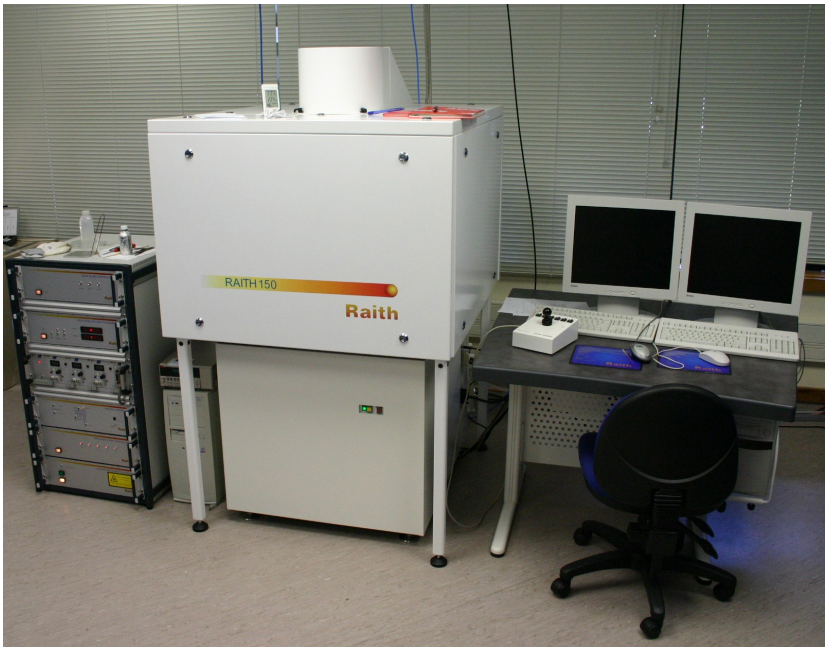

Figure 3.10 The recently installed Raith 150 in the UoC laboratory.

3.4.2 Raith 150

Later a new Raith 150 [42] was installed which had far superior performance to the ageing PSEM500. The beam drift is less than 100 nm/hour, beam current stable to better than 1%/hour, the stage position is accurate to ± 2 nm, and with stage leveling to allow for slight corrections to plane misalignments. The machine also features a cross-over free beam path, reducing the effect the electron charge has on beam disfusion. As well as system improvements, there were also software improvements. Large patterns are automatically split into their seperate write fields and written consecutively with no user intervention required. By having a very high precision stage, it was possible to very accurately correct the write field so that stiching errors were 20 nm or less. Unlike to the PSEM500, the write field was addressed via two 16-bit DACs, but this was multipled through two more sets of DACs to account for write field rotation and shape. The Raith could be operated at almost any magnification, but with larger write fields the beam became stigmatised towards the edges, and with very small write fields there were a large number of fields to expose. One of the better compromises is with a 100×100 μm^2 write field.

While this tool allows for native production and editing of GDSII (Graphic Data System II) patterns, it also supports importing of patterns through either GDSII, L-Edit or a ASCII text file formats. This allows for simple creation of repetitive and complex patterns.

3.5 DEVELOPMENT

When the resist is being exposed, either long polymer chains are being scissioned into shorter chains (positive resists) or short chains become cross linked into longer chains (negative resists). Development of resists is, in simple terms, a chemical bath that removes short polymer chains while leaving longer ones behind. The shortest chains dissolve into the developer first, followed by gradually longer and longer chains. If the development process is performed under the same temperature, time and concentration conditions, it becomes a very repeatable process. However if the development time varies from sample to sample, the exposure structures will vary in width, and likewise if the developer concentration or temperature changes, the speed at which the developer works changes. Development conditions can vary markedly from resist to resist.

3.5.1 PMMA

The development of the HMW/LMW bilayer PMMA resist is dependant on temperature and developer concentration. One of the popular developers used is methyl isobutyl ketone (MIBK) diluted in IPA at a ratio of 1:3 respectively. The PMMA sample are developed in the solution at 23 °C for 30 seconds, and then rinsed in IPA for a further 30 seconds, and blown dry with a nitrogen gun. To heat the solution to 23 °C, the beaker was held in ones hand until the required temperature was reached, and then the sample developed.

3.5.2 ma-N2403

Development of the negative tone ma-N2403 resist was performed in one of two developers produced and recommended by the resist manufacturer. It was found that the ma-D332 worked very well at room temperature (22 °C) when developed for 30 seconds. The rinse step was performed in water for 30 seconds, since any hydrocarbon based solvent would remove the resist.

3.6 METAL EVAPORATION

Since PMMA is a poor dry etch mask, a metal mask was used instead. The metal layer could be evaporated onto the sample at two different stages. If it is done before the resist is spin coated it can be used for an etch-back mask layer, or if done after resist development it was used as a lift-off etch mask. The two methods produce negative images of each other. The evaporator used was a Balzers BA510A, shown in Figure 3.11.

Thermal evaporation of materials is a very simple, yet highly effective means of coating samples. A schematic of a basic evaporation system is shown in Figure 3.12.

The samples to be coated are loaded face down in a holder located at the top of the evaporator. The material to be evaporated is loaded into a molybdenum aluminium oxide (MoAlO) boat which is placed into the evaporator and clamped between two electrodes directly below the samples. Once the chamber is closed and pumped down to a low pressure, around 2×10^{-6} Torr, a high current is gradually applied through the boat causing it to heat up. The metal in the boat first melts then begins to evaporate, and as the source area is small, all evaporated material effectively comes from a point source. Since there is little air in the chamber, the metal atoms travel in a very direct path from the source, coating everything in line of sight to it in a uniform manner. This means that any shadowed areas will have very little or no material deposited. This is useful in the case of lift off where the higher and lower regions of materials need to be separated. To help measure the amount deposited, a piezoelectric quartz plate is located inside the chamber, whose natural oscillating frequency changes depending on the type and mount of material deposited on it, so as more and more material is deposited, the higher its resonant frequency.

For the lift-off process the favoured metal alloy was nichrome, which has a very high dry etch resistance and could easily be removed by a wet chrome etch. This can be evaporated onto samples with relative ease, and only a thin layer is needed. This helps with lift-off as the thinner the metal is, the less likely it is to result in bridges that prevent lift-off from working well. For a 25 nm coating of nichrome the thickness monitor frequency increases by 1.0 kHz.

3.7 REACTIVE ION ETCHING

While wet etching has the disadvantage of generally being an isotropic etch (etches uniformly in all directions), reactive ion etching (RIE) uses a radio frequency (RF), 13.56 MHz, generated plasma which can be used to perform a very directional etch. All RIE work was performed exclusively in the UoC's Oxford Plasmalab^{80Plus} [43], pictured in Figure 3.13.

RIE, also known as dry etching, is a etching method which is performed at low pressures and often at low temperatures. RIE works by either sputtering or dissolving material by vapour phase gases, and allows for very anisotropic etches with almost vertical side walls. By controlling the etchant gases, temperature, pressure, gas flow rate and RF power it is possibly to fine tune etches to produce very specific and repeatable results. If a inert gas like argon is used, it is a primarily a sputtering type etch which produces very steep sidewalls due to the speed of the atom knocking the substrate atoms out. On the other hand, if oxygen (O_2) is used during etching it becomes a very dissolving etch as oxygen reacts with the substrate/masking material and removes in that manner. Oxygen etches organic material very quickly. The etch occurs in a very specific direction as the gas particles hitting the surface provide energy

Figure 3.11 Balzers BA 510 A Evaporator in the UoC laboratory.

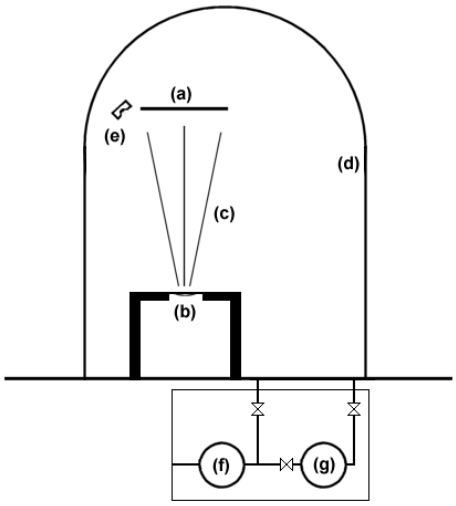

Figure 3.12 Schematic of an evaporation system. Samples are mounted facing downwards in the holder (a), while the material to be evaporated is loaded into a boat at (b). The chamber is closed (d) and pumped down to a low vacuum. When the pressure is low enough, current is passed though the boat (b) which heats up and melts the material in it. Once it is sufficiently hot, it will begin to evaporate and coat any surface visible to it. The piezoelectric quartz plate which monitors the amount evaporated is located at (e). The vacuum system is located below the chamber, which consists of a rotary backing pump (f) and a diffusion pump (g).

Figure 3.13 UoC's Oxford Plasmalab^{80Plus}. To the left is the liquid nitrogen dewer which is used to cool the electrode.

from their momentum. This momentum is most significant coming straight down onto the surface, due to the nature of the RIE process.

Figure 3.14 illustrates how an RIE system works. The gas mixture is controlled by a mass flow controller (MFC) for each of the three lines externally and is let into the chamber at (a). At (b) the gas joins the plasma where free electrons ionise it. These charged ions are accelerated vertically up and down by the 13.56 MHz RF voltage (c) applied to the base plate. These ions, when they hit the sample surface (d), can either bounce off the surface or etch it by reacting with surface atoms or physically bombarding them. This results in atoms being removed and the etching process. If an area of the substrate is masked, the free ions are unable to hit the surface and etching will be prevented, however the mask itself will be etched somewhat. The system pressure is controlled by the automatic pressure control (APC) valve located at (e). The electrode temperature is controlled by either heating by electrical element or cryogenic cooling by liquid nitrogen.

Dry etching of Si_xN_ysubstrates was performed by using CHF_3 in combination with either O_2 or Ar gases. Ionised CHF_3 produces free F^- ions as per Equation (3.6), which in turn chemically etch Si_xN_ysubstrate by the the process showing in Equation (3.7) to produce tetraflurosilane and nitrogen gases. Polymer build ups on the surface from products of etching must also be continually removed to allow etching to proceed well. For this either O_2 or Ar was used. O_2 works by chemically attacking the polymers, but

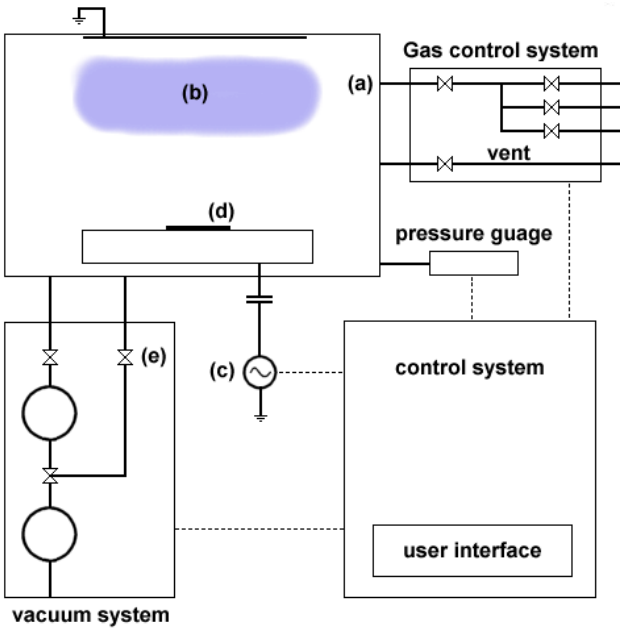

Figure 3.14 How the RIE process works. Gas mixture is let in through (a), ionised and RF excited forming a plasma (b). Ions get accelerated up and down by the RF generator (c), and bombard the sample surface and so etch it at (d). The APC valve (e) which controls the amount of exhaust gases pump out of the chamber.

also attacked the resist, meaning a decrease in the possible selectivity. Ar is an inert gas, and so can only remove the polymers by physically bombarding them. While it also attacks the resist, it does not do so with the vigour of O_2.

$$e^- + CHF_3 \rightarrow CHF_2^+ + F^- + e^- \tag{3.6}$$

$$Si_3N_4 + 12F^- \rightarrow 3SiF_4 + 2N_2 + 12e^- \tag{3.7}$$

Some basic methods of adjusting etch recipes is outlined here. By reducing the etch pressure, the majority of the atom movement is purely in the vertical direction, meaning that most of the etching is done straight down into the substrate. By using a higher pressure, atoms will knock into one another much more often, and hence their movement will be more unidirectional. This allows for etches that will allow for some rounding/reducing of details, producing a smoother result. Higher etching power means more acceleration vertically of the ions, producing a more anisotropic etch. The size of the structures being etched also affect the etch rate, with smaller structures being etched at a lower rate. This is due to the smaller angle of entry for high energy ions to enter the cavity.

3.8 SPUTTERING

Sputtering is another technique for coating substrates with metals and other materials. Sputtering has advantages over evaporation in that it can sputter materials that cannot be evaporated such as tungsten, and also allows for the introduction of reactive gases during sputtering to produce other substrates (such as using a zinc source and oxygen gas to produce piezo electric ZnO coating, or silicon source and nitrogen gas to produce Si_xN_y).

Figure 3.16 illustrates how a DC magnetron sputtering system works. Sputtering works by producing a plasma above a source target material. The plasma is contained above the target by a magnetic field. Argon is normally used for the plasma while other gases such as nitrogen and oxygen can be introduced into the chamber if their inclusion is desired in the deposited film. This plasma bombards the target surface knocking atoms off which leave the surface in random directions and coat the chamber fairly uniformly. The sample, located above the target, receives a portion of this coating, and to ensure it is more uniform, the samples are often rotated in the chamber during the process. A crystal plate monitors the deposition and the growth is displayed on a readout in nm, provided the correct tooling factor is used. The UoC sputter is a BOC Edwards Auto 500 with DC/RF sputtering and electron beam evaporation [44], shown in Figure 3.15.

3.9 PATTERN TRANSFER TECHNIQUES

Transferring the pattern from developed resist into the Si_xN_y substrate could be done using one of two main methods. The two main methods of transferring the pattern from the resist to metal are lift-off and etch back.

3.9.1 Lift-Off

With the lift-off method, the metal is evaporated on top of the patterned resist. The metal coats a very uniform layer covering both resist and the underlying layer where the resist has been developed away. If evaporated well these two areas will be separated by a vertical distance and metal on the resist should be easily removable by dissolving the resist. This only then leaves the resist in contact with the substrate. For lift off to work well, the resist profile edges should be very sharp, or better yet overhanging. If the edges are graduated the two metal layers are joined by continuous metal, so it now becomes impossible to remove the resist which is fully enclosed by the metal. Overhanging resist features can be produced by using a multi-layer resist structure with the lower layer being more soluble in the developer. The metal needs to evaporated vertically down onto the surface to produce the best results. It can be used at an angle

Figure 3.15 BOC Edwards sputtering system in the UoC laboratory.

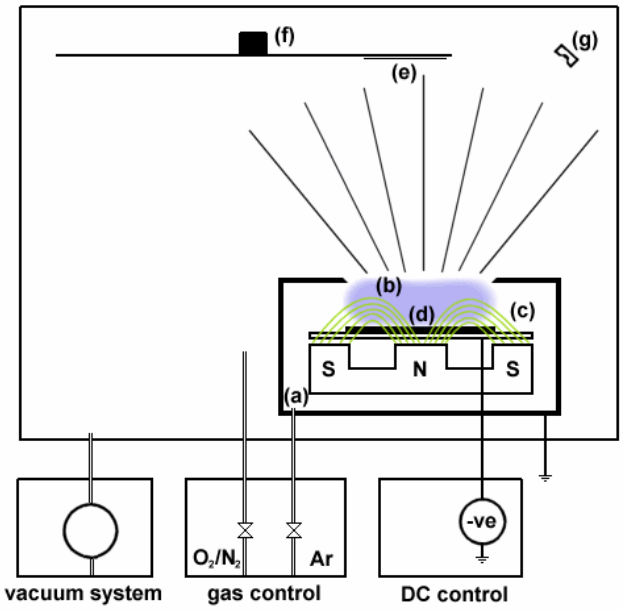

Figure 3.16 How a DC magnetron sputtering system works. The Ar gas is let through (a), where it enters the plasma (b) which is contained in the magnetic field (c). The plasma knocks atoms off the source target (d) which uniformly coat all surfaces in line-of-sight, including the sample (e). The sample can be rotated around the chamber by turning the sample holder (f). The deposition is monitored by a piezoelectric crystal (g).

to produce very small over lapped areas of differing metals. Figure 3.17 shows the main process steps of creating an etch mask and etching into the substrate.

3.9.2 Etch Back

Etch back has a advantage over lift-off as it requires less steps and does not suffer so badly when the resist layer is not so well formed. Etch back works by the resist acting as an etch mask for either directly etching the substrate, or etching an intermediate etch barrier which is in turn used as a mask for etching the substrate. While this can be a wet etch, dry etching is more frequently used as it can produce a more anisotropic profile.

3.9.2.1 Indirect Etch Back

By using an intermediate etch barrier one can overcome a resist's poor etch selectivity. The resist is used to mask the etch barrier in the initial etch step, then the process is changed to one that etches the substrate preferentially to the etch barrier. By using this technique one is able to use almost any resist, even if it has a poor etch performance, to etch deep features into the substrate.

For this method to work the etch barrier layer needs to be applied prior to the

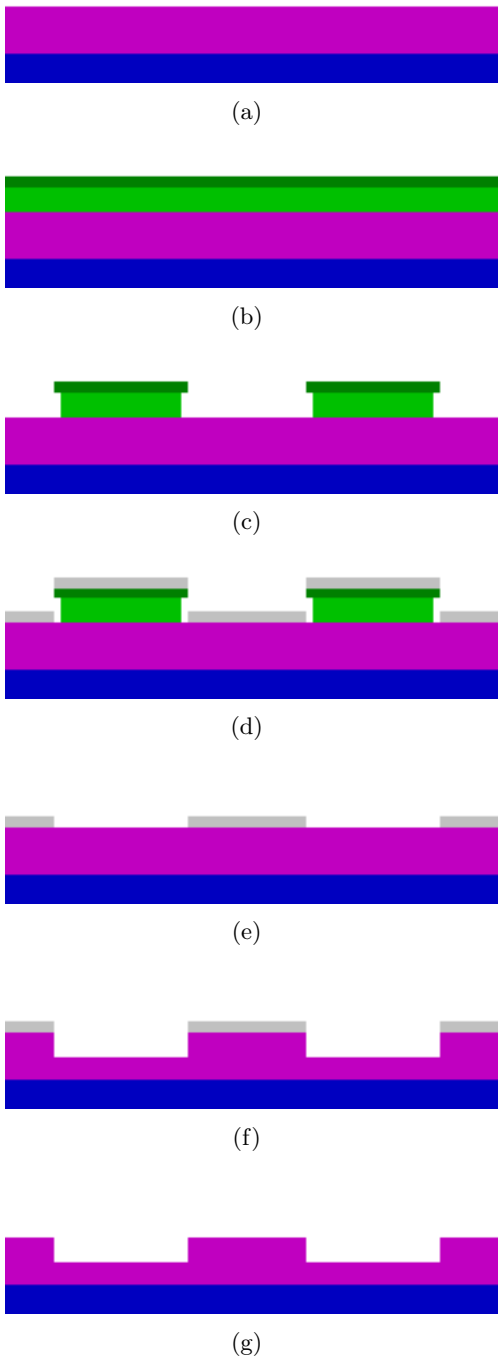

Figure 3.17 Pattern transfer by lift-off. (a) clean sample is coated with a bi-layer resist (b), patterned and developed (c), metal is evaporated on top of remaining structures (d). The remaining resist/metal structures are removed by solvent (e). The metal pattern left is used as a dry etch mask (f), which is stripped afterwards giving the final result (g).

resist. The etch barrier can be a spin on coating, or a metal evaporated or sputtered onto the substrate. Since this layer is required to be level and uniform, the metal can be applied by sputtering allowing for metals which cannot be easily evaporated, or at all, such as tungsten. Figure 3.18 shows the main process steps for etch back.

The resist is then coated over the etch barrier, patterned and developed. This resist layer is then used as a mask to etch the etch barrier, which in turn is used as a mask as well to etch the underlying layer. This has the advantage that the sample does not need to be removed from the RIE during the process - only the process gases need to be changed.

3.9.2.2 Direct Etch Back

This technique requires the least extra processing, however does have a few disadvantages to etch back procedure as described in the Section 3.9.2.1. Since the only mask is the resist itself, it must have a very sharp side wall profile if it is to create binary type structures, and must also have a high selectivity and be thick enough to not be fully removed during etching. If a suitable resist is found as an etch mask, this is the quickest and most accurate technique. This is the only useful technique for transferring 3D resist structures into the substrate, as it does not rely on binary masking. Figure 3.19 shows the main steps for this process.

3.10 NANOIMPRINTING

Imprinting was performed by the hot embossing method. This approach was chosen for its simplicity. The press used was the UoC built one shown in Figure 3.20. The mold and sample were placed facing each other into the recess in the press. The press was then wound down 9 full turns so that a spring was compressed by 9 mm, which equated to a force of 1,000 N. Since 10×10 mm^2 samples were used, that equated to a imprint pressure of 100 bar. The press was then placed on a hot plate which was heated to 80 °C. After 20 minutes, the press was removed from the hot plate and quenched in 20 °C DIW for 2 minutes. The press was blown dry by N_2 gun and the sample and mold removed.

3.11 INSPECTION TECHNIQUES

To check the results of fabrication steps, a number of inspection techniques were employed. The primary technique used was optical microscopy, as it was the fastest method in which to obtain basic information about the sample. Since its resolving technique is limited, further inspection was performed by either atomic force microscopy

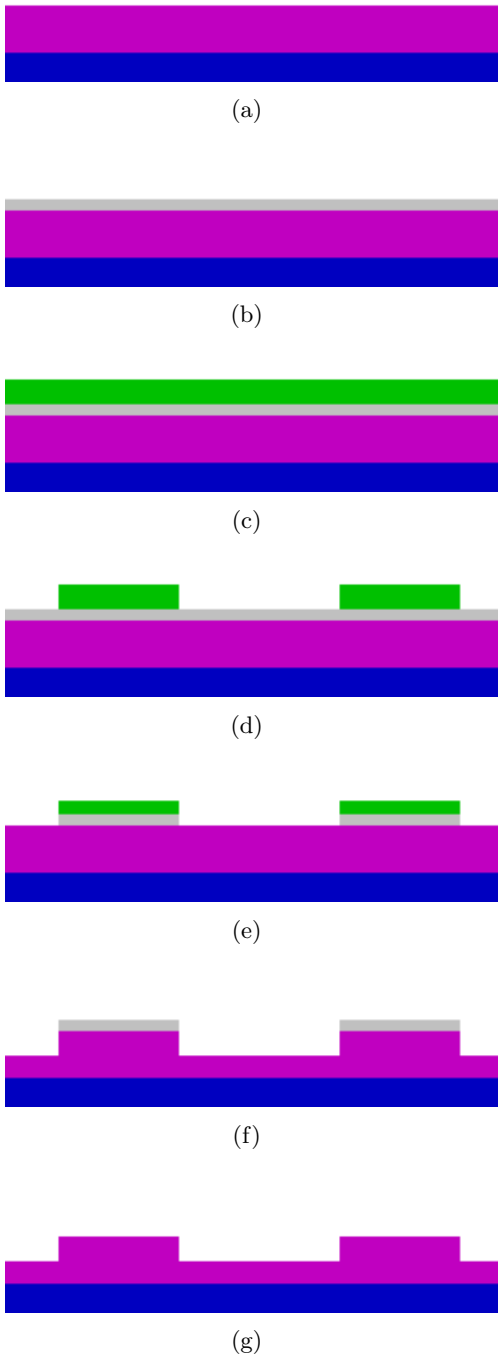

Figure 3.18 Pattern transfer by etch-back. A clean sample (a) has an etch barrier layer applied (b), followed by a resist layer (c). The resist is patterned and developed (d). The resist is then used as a mask for dry etching the etch barrier (e). The dry etch chemicals are then changed and the etch barrier is used as a mask to etch the substrate (f). The remaining etch barrier is then stripped giving the final result (g).

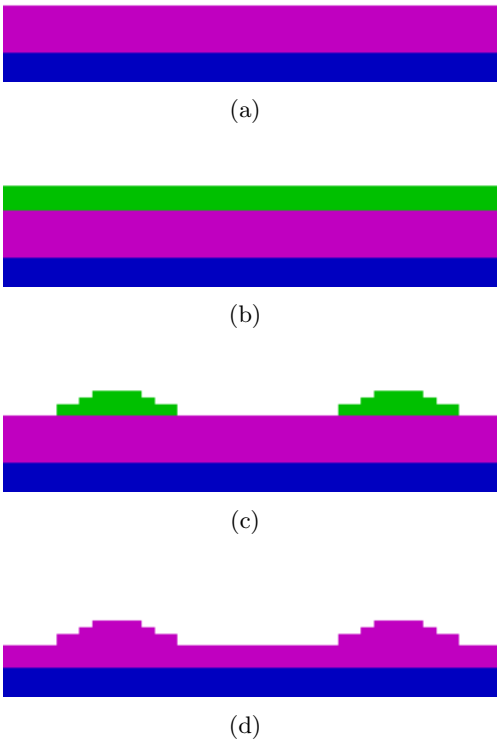

Figure 3.19 Pattern transfer by direct etch-back. A clean sample (a) is coated with a resist layer (b), 3D patterned and developed (c). The pattern is then dry etched back into the Si_xN_y substrate, accurately reproducing any 3D structure, and cleaned if necessary. The resist can also be used as a purely binary mask to create 2D structures.

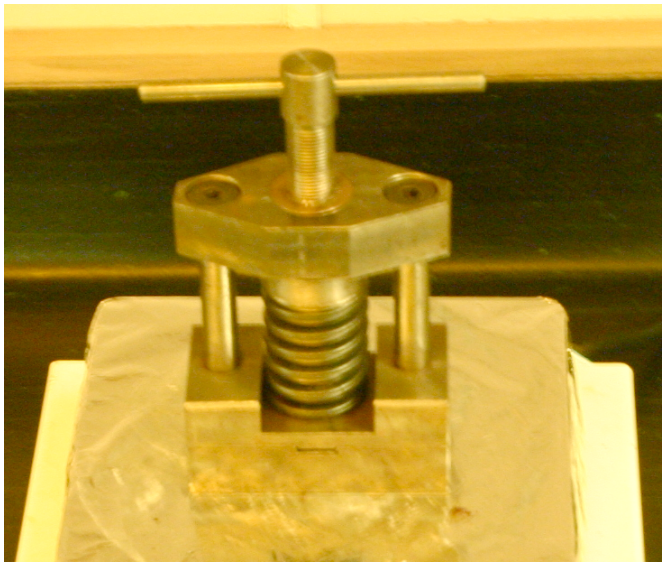

Figure 3.20 The UoC built imprint press on a hotplate.

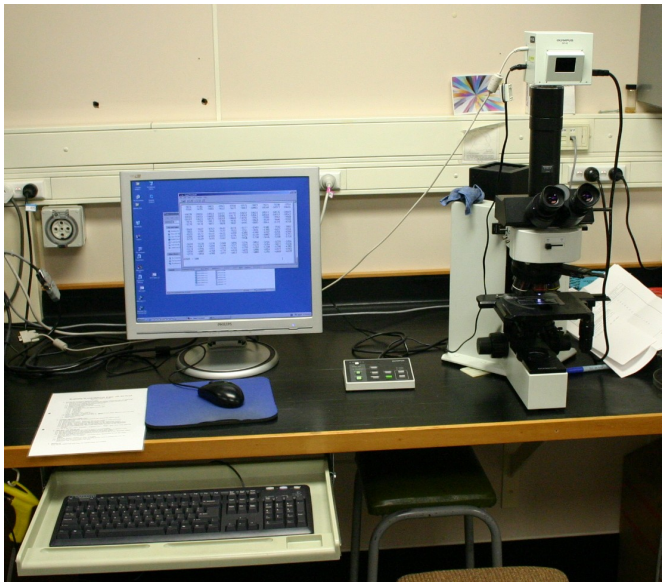

Figure 3.21 Olympus BX60 Optical Microscope with a DP10 digital camera attachment.

(AFM), or scanning electron microscopy (SEM). Each method has its own advantages and disadvantages, and no one technique could replace the other methods.

3.11.1 Optical Microscopy

Optical microscopy was almost always used first. While it did not provide high resolution images, it was a very fast method by which an good overall picture of the sample could be taken. Areas could be noted for further inspection by AFM or SEM. The smallest structures visible by the microscope had a period around 1 μm. The main limitation to this technique is the wavelength of visible light. The microscope can be seen in Figure 3.21, which had a digital camera so images could be loaded directly into the computer.

3.11.2 Atomic Force Microscopy

AFM was primarily used for profiling the surface down to the nanometre scale. By scanning a resonating tip across surface the machine could determine how far the tip was from the surface by the amplitude of the resonance. The tip deflection was measured by a laser spot that was reflected off the tip cantilever, so minute movements were greatly amplified before reaching the detector. The tip was then moved up or down so that the amplitude remained constant. By knowing how much the tip had been moved up and down, a very accurate profile of the surface was obtained. The vertical resolution of the system is accurate to 0.05 nm, and laterally to 2 nm. Since piezo columns have a little hysteresis, only scans in a certain direction were used, while the scan information of the return path was ignored. The AFM used, a Digital

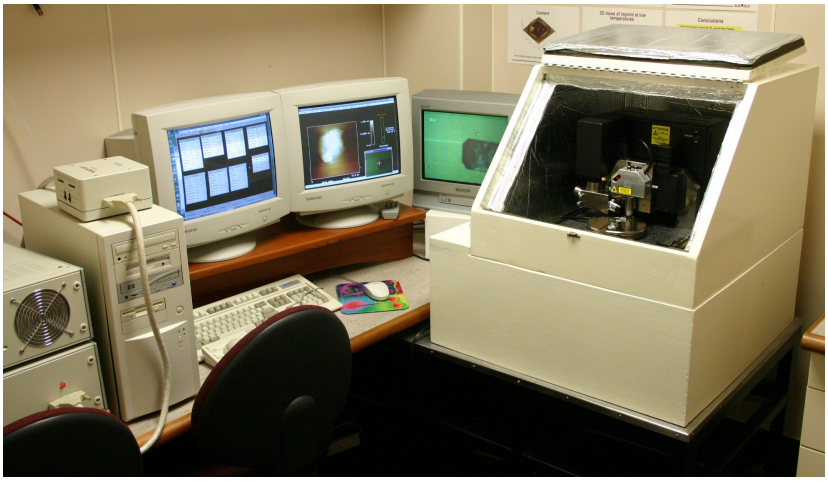

Figure 3.22 Digital Instuments (Veeco) DI3100 Atomic Force Microscope installed in the UoC laboratory. AFM works by using a piezo column to scan a small tip across the sample surface and detects one of any number of properties some of which includes profile, elasticity, adhesion, and magnetic/electric field.

Instruments (Veeco) DI3100, is shown in Figure 3.22 sitting on a low vibration table enclosed in a UoC built acoustic shield. Since scanning is a serial process, the scanning of a image frequently took up to 10 minutes each. This is significantly slower than any other inspection technique used in this study.

3.11.3 Scanning Electron Microscope

Scanning Electron Microscopy (SEM) works very similarly to EBL as it is described in Section 3.4. By measuring the reflected electrons, it is possible to build up an image of the substrate. Typically, more electrons are reflected from sharp edges and insulating substrates due to the charging effect. More electrons stay in these areas for longer, eventually building up enough charge so that that part of the substrate reflects more electrons. All SEM work was performed on the RAITH150, shown in Figure 3.10.

While the SEM could quickly take very high resolution images, it was limited in that it could not provide much information regarding the material being examined, except changes in the charging level. Significant time was also consumed loading and unloading samples into and out of the tool. However if samples were sectioned and the profile examined, a lot of detail was available which was unobtainable by other means.

3.12 SUMMARY

This section has described the methods used to produce nanoimprint molds by two different means. Firstly though using a metal mask and indirect etch back to produce 2D structures, and secondly by using a tone resist capable of producing 3D structures in a single step. Resist spin coating, e-beam patterning, development, reactive ion

etching, sputtering basics have been covered. Inspection techniques have been outlined to show the benefits and shortcomings of each system, and illustrating that there is no 'best' method.

Chapter 4

MOLD FABRICATION

4.1 OUTLINE

This chapter deals with the actual processes and development steps undertaken to produce the silicon nitride molds used in this study. First covered is the fabrication of 2D molds by use of the older PSEM500, and then the progress onto the Raith150 and 3D molds. Investigations into resist coating and curing, EBL writing resolutions and exposure densities, dry etching and anti-adhesion coatings have been performed.

4.2 TWO-DIMENSIONAL MOLDS

The fabrication of two dimensional molds was performed first. While processing performed here is a little more involved than that for the 3D molds, the reliability of results was somewhat better. By using a metal mask via lift-off or indirect etch back, very sharp and deep features could be achieved in the RIE. Both lift-off and indirect etch back techniques were investigated.

4.2.1 Sputtering

Indirect etch back used a thin tungsten coating sputtered on top of a clean substrate. This allowed for a very uniform layer so that the resist could be spin coated without streaks or thickness variations. The sputtering process began with taping the samples on the rotating holder with aluminium tape, and loading it into the top of the chamber. The tungsten sputtering target was placed in the DC sputtering source. The chamber was then closed and pumped down to 2×10^{-5} mbar. The Ar gas inlet was opened, the flow rate set and the plasma struck. The plasma was left going for 5 minutes prior to opening the shutter to allow for the removal of impurities from the target surface. The sample holder rotator was started, and then the shutter was opened for the specified time. Once the process was complete, the plasma was shut off, the chamber vented with N_2 and the samples unloaded. The sputtering process parameters were set to those shown in Table 4.1.

Table 4.1 Process parameters for DC magnetron sputtering of tungsten.

Process	W deposition
Gas 1: flow rate (sccm)	(Ar) 10
Target type	Tungsten (W)
DC power (W)	200
Chamber Temp (K)	303
Shutter open time (s)	50
Deposition rate (nm/min)	11.5

4.2.2 Resist Coating

Samples were diced, cleaned and PMMA spin coated as per Sections 3.2 and 3.3.1. The dual layer PMMA resist stack performed well and no changes were required from the UoC standard processes. Soft-baking after each resist coating produced no observable defects in the resist surface, and none appeared at any further stage of fabrication due to the resist quality.

For those samples that were used for indirect etch back, only a single coating of HMW PMMA was applied over the tungsten layer. Because of the thin resist, with a metal layer beneath it, the potential resolution was higher due to less forward scattering. The tungsten layer also helped to prevent charging during EBL by conducting electrons away from highly charged areas.

4.2.3 Electron Beam Lithography

While the resist coating method stayed the same throughout the process fine tuning, the e-beam lithography process went through a number of development steps. This was done twice, initially for the PSEM500, but again later when the Raith150 was available, and all e-beam lithography shifted to that system. The four areas of interest when developing the process were: writing voltage, exposure dosage, beam size (or aperture size) and pixel spacing.

Patterns were all initially generated in L-EDIT, exported into a CIF file and then converted by a user program into a format usable by the PSEM500. The UoC developed user program had very limited support for rectangles only. This was totally rewritten to fully support all documented features of the CIF format, excepting only text objects, so that polygons could be used along with rotation, translation and instances of grouped objects. This greatly eased the development of patterns. A viewer program was updated and allowed the EBL files to be examined prior to writing.

On the PSEM500, all patterns were written at 50 keV, and several tests were performed to confirm the given value of 600 μC/cm^2 as an adequate clearing dosage. Features became distinguishable at around 500 μC/cm^2, with most, but not all, fully developed out at 550 μC/cm^2. 600 μC/cm^2 ensured total exposure of the PMMA film

with no unwanted remnants. The beam spot size used was normally 16 nm, the best compromise between beam current, speed and resolution. Using a smaller spot size resulted in much lower beam currents and longer writes, but no increase in potential resolution. The normal magnification used was 2,500×, which had a write field size of 57.8 × 38.7 μm, meaning the minimum address spacing possible by the 12-bit DACs was 14.1 nm in the x direction and 9.5 nm in the y. If large patterns were desired, a larger magnification had to be used, as write field stitching was extremely inaccurate, and likewise if higher resolution patterns were desired, 5,000× magnification was used. Higher magnifications than this were not used as the 6.9 × 4.5 nm pixel spacing was higher than the obtainable resolution from PMMA or the e-beam system.

4.2.4 Development

Pattern development occurred as per Section 3.5.1. With the bilayer PMMA stack, the LMW is more soluble than the HMW, and so dissolved faster, leaving the HMW layer overhanging the LMW layer, creating a good undercut profile for lift-off. On the single HMW layer samples, the features are directly on the tungsten layer and so more stable. This is especially important for very small bilayer structures which could become so undercut that they detached from the substrate.

4.2.5 Lift-off Processing

This subsection concerns itself with the transfer of the patterns from the developed resist into the Si_xN_y substrate by the lift-off process. This includes the metal evaporation, lift-off itself, reactive ion etching and cleaning.

4.2.5.1 Metal Evaporation

Before evaporation took place, the chamber occasionally needed cleaning. This consisted of removing all loose metal flakes from the chamber and checking the o-ring seal was clean to ensure a good vacuum. The samples were loaded into the top of the evaporation chamber, and the MoAlO boat had some freshly cut high purity nichrome wire added. The boat was clamped between the electrodes, and the chamber shut. The rotary vacuum pump was then started, and hot water pumped through the evaporator cover water jacket. This is to heat up the chamber interior, and raise the pressure, thereby making it easier to pump down. Once the vacuum was great enough, the machine automatically switched to a diffusion pump that was backed by the rotary pump. After 30 minutes the hot water was turned off, and cold water applied. This is used to cool the chamber, thereby lowering the pressure and allowing some contaminants to stick the chamber walls. Once the pressure had reached 2×10^{-6} Torr, the evaporation was ready to begin. The current through the boat was gradually increased over

Table 4.2 Reactive ion etch recipie for Si_xN_y with a NiCr mask.

Process	Ar etch
Gas 1: flow rate (sccm)	(CHF_3) 30
Gas 2: flow rate (sccm)	(Ar) 25
Electrode type	Nichrome
Temp (K)	253
Time (min)	5
Etch pressure (mTorr)	20
Si_xN_y etch rate (nm/min)	40

a 5 minute period. This was ensure that the boat did not heat up too rapidly and break. The thickness monitor had its frequency zeroed, and the shutter opened. The evaporation took place over a 5 - 10 minute period during which the frequency monitor increased by 1 kHz, indicating that 25 nm of nichrome had been deposited. When the 1 kHz increase had been obtained, the shutter was closed and the heating current turned off. The samples were removed after the chamber had been vented back to atmospheric pressure.

4.2.5.2 Lift-off

To remove the extraneous metal that was deposited on top of the PMMA, the sample was placed in an acetone bath for a period of time to perform the lift-off step. This removed all the remaining PMMA and the nichrome that had been evaporated on it. Gentle agitation by hand, squirting acetone with a disposable pipette or by using the ultrasonic bath was found to speed the process up, however pattern definition was always poor afterwards, especially for small features. It was found that by leaving the sample in acetone undisturbed for an extended period of up to one day, the lift-off performed well. Care had to be taken to ensure that there was always enough acetone in the bath, as it evaporated off fairly quickly.

4.2.5.3 Reactive Ion Etching

A single dry etch recipe, developed by a previous study performed at the UoC laboratory [17], was used on the Si_xN_y substrates. The process parameters are listed in Table 4.2. The etch performed well producing 200 nm high features with smooth vertical side walls. It was determined that no variation to the initial recipe was required, as it met the standards required.

4.2.5.4 Substrate Cleaning

To clean the substrate of all contaminants, the sample was first washed in a chrome stripper (1 part HCl, 1 part HNO_3, 3 parts DIW) to remove the nichrome etch mask,

Table 4.3 Reactive ion etch recipe for indirect etch back with PMMA on tungsten on Si_xN_y.

Process	W etch	Si_xN_y etch
Gas 1: flow rate (sccm)	(SF_6) 80	(CHF_3) 30
Gas 2: flow rate (sccm)	-	(Ar) 25
Electrode type	Nichrome	Nichrome
Temp (K)	293	253
Time (s)	7	120
Etch pressure (mTorr)	100	20
Etch rate (nm/min)	(W) 280	(SiN) 40

and then cleaned by acetone, methanol and then IPA in the ultrasonic bath for five minutes each to remove any scum or debris which had accumulated in the etch process. The sample was blown dry by N_2 gun and dried further in the 95 °C convection oven for 30 minutes.

4.2.6 Etch Back

This subsection concerns itself with the transfer of the patterns from the developed resist into the Si_xN_y substrate by the indirect etch back process. This includes the two stage reactive ion etching and cleaning.

4.2.6.1 Reactive Ion Etching

Two etches were used to perform the indirect etch back. The first etch, to etch the pattern through the tungsten, was a quick high pressure etch using only SF_6. The subsequent etch used the tungsten as a mask and transferred the pattern into the Si_xN_y substrate using CHF_3 and Ar. The etch temperature and pressure were lower and hence the etch rate was considerably slower, allowing for a anisotropic etch with smoother sidewalls. In between the two etches, the gas lines were purged to remove any remaining SF_6, and the chamber was pumped down to remove as many other contaminants as possible. The process parameters for both etches are shown in Table 4.3.

4.2.6.2 Substrate Cleaning

To clean the Si_xN_y substrate after a etch back procedure a two step process was used. Firstly the sample was cleaned by acetone, methanol and then IPA in the ultrasonic bath for 5 minutes each to remove any possible remaining PMMA or other easily dissolvable materials. This was followed up by a 10 minute hydrogen peroxide etch (30% H_2O_2) [45] to strip the tungsten mask layer, rinsed in DIW and blown dry using N_2.

4.3 THREE-DIMENSIONAL MOLDS

By their nature, 3D patterns are difficult to produce well. If, for instance, a binary resist is used, several exposure/developing/etching steps are required. Not only does this take a significant amount of time, but there is a greatly increased chance of failure due to the increased number of steps and alignments. By producing the 3D structures in a single step, minimal alignment errors are encountered. This was made possible by using ma-N2403, a negative tone DUV and EBL resist.

4.3.1 Resist Characterisation

While the ma-N2403 resists data sheet showed good performance, little information was provided on the details of processing it. So to become useful, the resist had to be characterised. This included spinning speed and time, exposure dosages, pre-baking, development process and etch selectivity.

4.3.1.1 Resist Coating

When spin coated onto the Si_xN_y substrate at 4000 RPM for 1 minute, the resist ma-N2403 resulted in a film thickness of 300 nm. This was measured by scratching the resist with a fine point and then scanning the resultant trench by AFM. This was only possible on Si_xN_y substrates due to its hardness. A Si substrate might have been scored, misrepresenting the thickness of the resist. By thinning the resist with the ma-T1024 thinner, produced by the same manufacturer, at a 1:1 ratio by volume, the thickness dropped to 75 nm. This allowed for higher resolution from the resist by reducing the area that forward scattering effects. However it was found when small features were being produced, they would often detach from the substrate and end up located elsewhere. An example of this with missing and moved characters is shown in Figure 4.1. The solution to this problem involved the use of a resist primer to increase adhesion to the substrate. HMDS was used for this task, and once its use had become standard, no further small structures were found to have detached and moved.

Another alternative method preventing small structure movement was found when a sample had been left in sunlight. Since the sun is a source of UV light, and the resist is also DUV sensitive, the sample had had a small uniform unquantified DUV exposure. It was found that this sample had a small amount of resist remaining in 'unexposed' areas after development which provided a base on which all the small structures were part of, and thereby could not detach from the surface. It is proposed that a low DUV exposure can also reduce the occurrence of small features detaching, however this was not investigated further as a workable solution had already been found.

Once the resist thickness was measured, a number of exposures were performed on samples that were written while varying the acceleration voltage, soft-bake method and

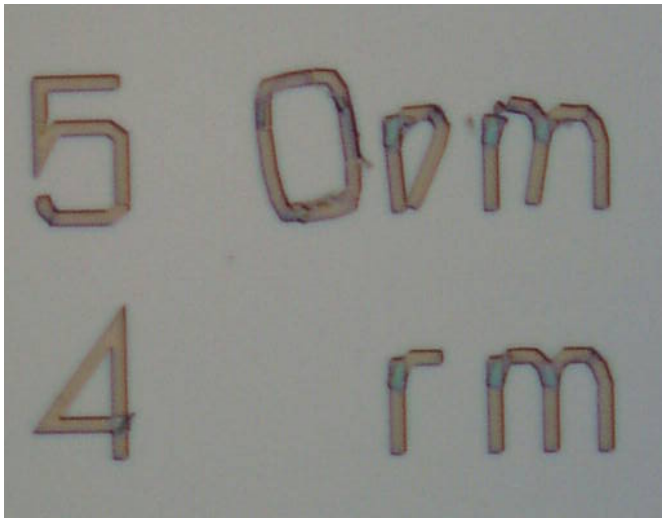

Figure 4.1 Missing, moved and distorted resist structures, due to a lack of resist adhesion to the SiN substrate. The top line should have been '500nm' and the bottom '400nm'. The adhesion problem was counteracted by using HMDS resist primer.

base exposure dosage. The most informative results of these tests can be seen in Figure 4.2. As can be seen, (b) has the worst exposure out of all the samples. Similar results occurred to all samples which had been soft-baked by hotplate. Samples (a), (c) and (d) had all been soft-baked for 30 minutes in the 95 °C convection oven, and provided much better results. This technique then became part of the standard production process.

4.3.1.2 Electron Beam Lithography

To pattern the 2D and 3D structures, a single pass e-beam write was performed. By doing the write in a single pass, inter-write alignment steps were not required, and so allowed for simpler processing.

The ma-N2403 resist is a negative resist, so unlike PMMA it cross links when exposed, creating larger insoluble polymer chains. The higher the exposure dosage, the more resist is cross-linked, leaving larger structures after development. When a tightly focussed beam is used, the majority of the cross linking occurs directly in the beam's path, so the structures will generally grow taller rather than wider with increasing dosage. By increasing the dosage far beyond that required to expose the resist full thickness, the proximity effect will begin to expose the surrounding areas, and the structures will grow laterally.

A number of test patterns were used to check the performance of the procedures developed. Initially the Raith test pattern (Figure 4.2) was used to get the rough parameters, and best acceleration voltage. Amongst the other results for samples written at acceleration energies of 10 keV (a), 20 keV (c), and 30 keV (d). The best and most consistent results were obtained while writing at 10 keV, so it was made part of the exposure regime.

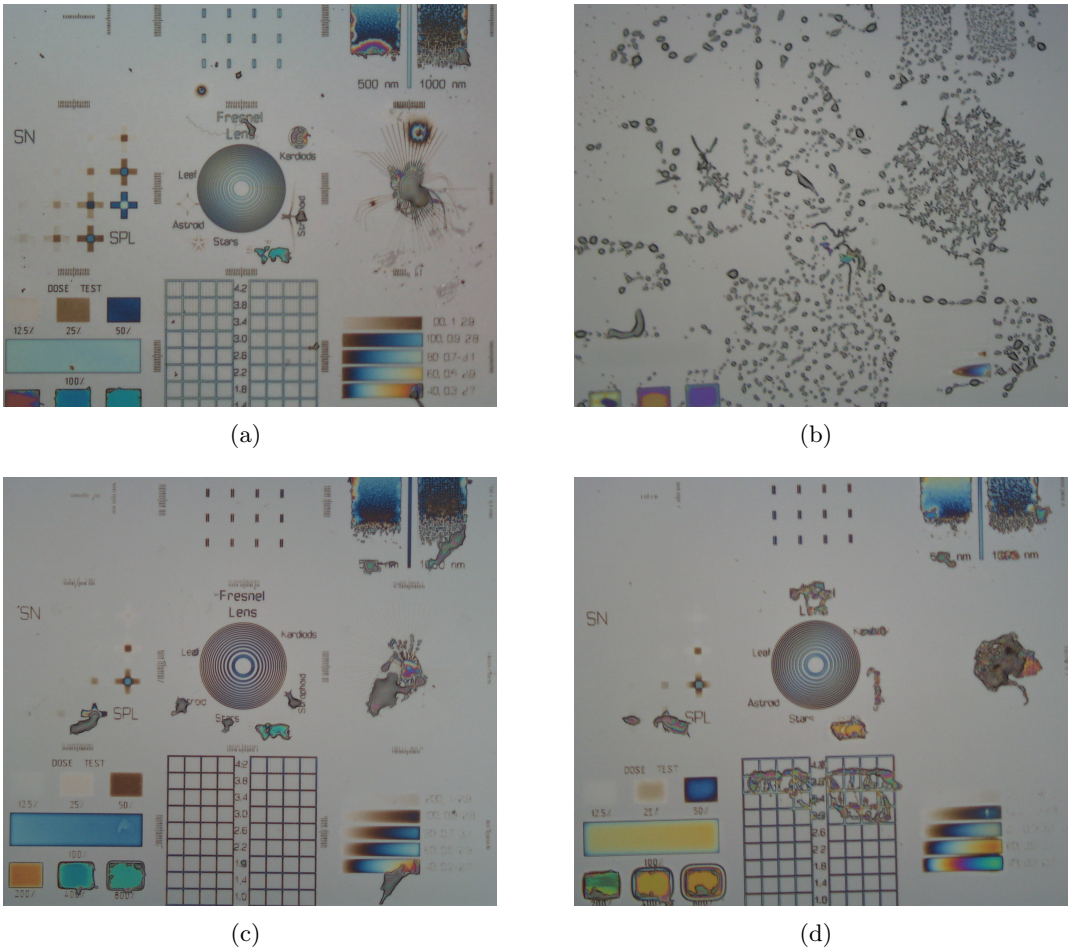

(a) (b)

(c) (d)

Figure 4.2 Test pattern results for ma-N2403 without the use of a resist primer. (a) Pattern exposure at 10 keV, with a nominal exposure dosage of 10 uC/cm^2 but was soft baked in a convection oven at 95 °C for 30 min prior to exposure while (b) was soft baked at 95 °C on a hotplate for 60 s. (c) was written at 20 keV, with a nominal dosage of 20uC/cm^2 and (d) 30 keV with dosage of 40uC/cm^2. Both (c) and (d) were soft-baked in the convection oven. The imaged area is approximately 300 μm wide.

Figure 4.3 New Zealand test pattern. This three-dimensional map of New Zealand was used as a test pattern to test the EBL procedure performance. The darker areas had a higher exposure dosage than the lighter areas. This was written at various scales ranging from 6 to 300 μm in width.

Fine tuning of the exposure process was performed using several patterns, one a 3D map of New Zealand, shown in Figure 4.3, and others shown in Figure 4.4. The 3D map provided a pattern with innumerable different features of various sizes, shapes and heights, providing a very difficult 3D pattern to expose well. The other patterns, were more structured and were used to provide a more quantitative evaluation of the exposure process.

Over a number of exposures, it was determined that the resist had a high resolution capability and was very sensitive to exposure. This however also led to its own difficulties. Since the nature of a scanning e-beam system is that it exposes a single pixel at a time, the dwell time for each pixel was very short. Using the standard 30 μm aperture on the Raith150, the beam current was around 230 pA, and so for a exposure dosage of 10 μC/cm^2 at 10 nm pixel spacing the dwell time needed to be 830 ns. While this was not beyond what the system could perform, the timing steps where done at 200 ns intervals (a 5 MHz controller), so fine dosage adjustment was not possible. By going to a smaller aperture, and hence a lower beam current, finer control was realisable. Two smaller apertures, 20 μm and 10 μm had an average beam current of 125 pA and 33 pA respectively, producing longer dwell times as shown in Table 4.4. The 20 μm aperture was used in conjunction with the 20 nm pixel spacing for most of the work.

Problems were encountered while writing high resolution patterns. This was a result of the Raith 150 automatically performing the pixel stepping inside polygons,

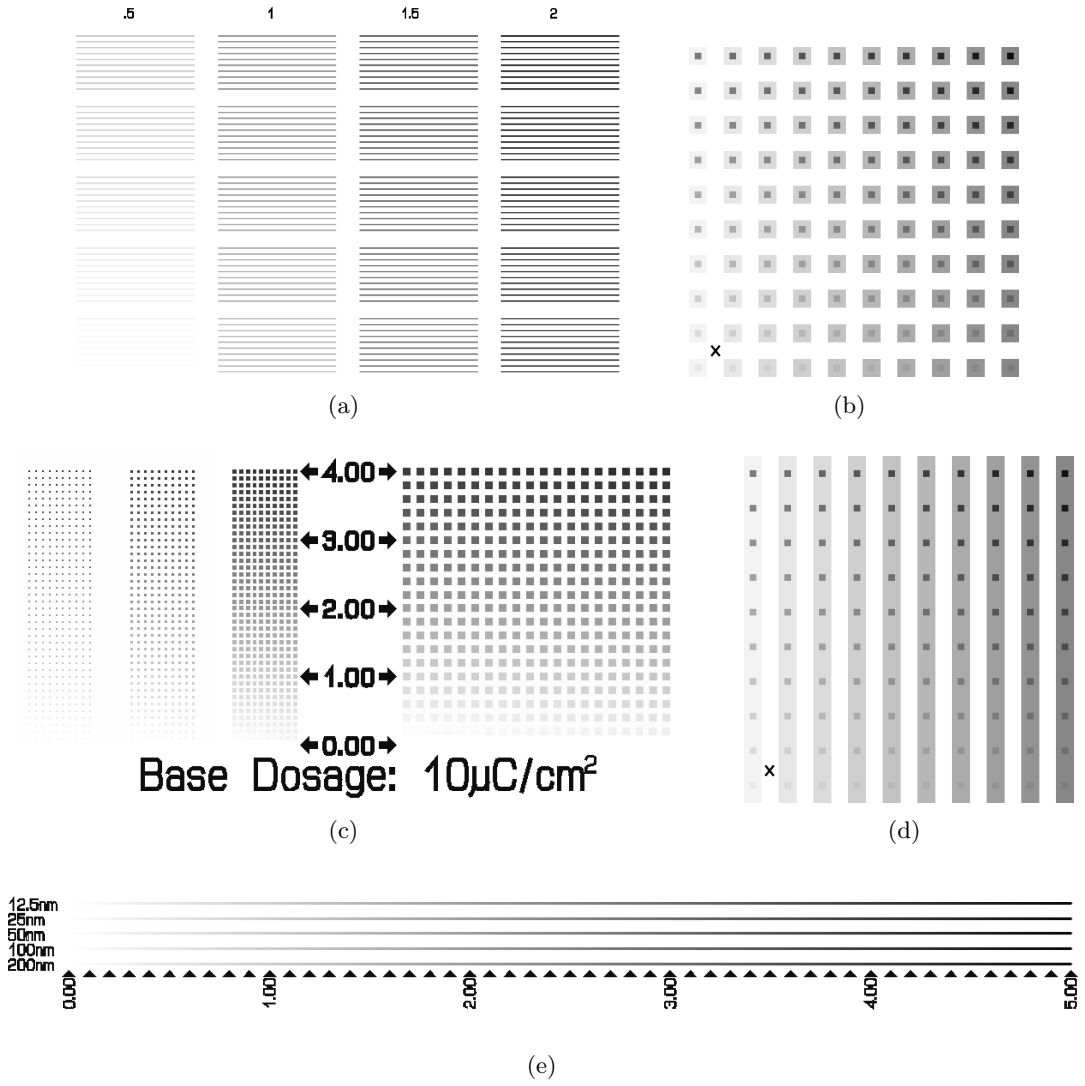

Figure 4.4 A number of test patterns used to check the EBL procedure. (a) A dose test with dosages varying from 0.1 μC/cm^2 to 20 μC/cm^2, (b) another dose test vary from 0.01 μC/cm^2 to 40.0 μC/cm^2. Squares in squares (c) and squares on lines (d), dosages varying from 0.1 μC/cm^2 to 20.0 μC/cm^2. (e) Dose test for lines of single pixels. Dosages vary from 0.1 fC/pixel to 5.0 fC/pixel, while pixel spacing varied between 12.5 nm to 200 nm. Patterns are not shown to relative scale.

Table 4.4 Relationship between aperture size, beam current, pixel spacing and dwell time to obtain a dosage of 5 μC/cm^2 at 10 keV.

Aperture Size (μm)	Beam Current (pA)	Pixel Spacing (nm)	Dwell Time (ns)
10	33	4	606
		10	3,790
		20	15,200
20	125	4	160
		10	1,000
		20	4,000
30	230	4	87
		10	429
		20	1,720

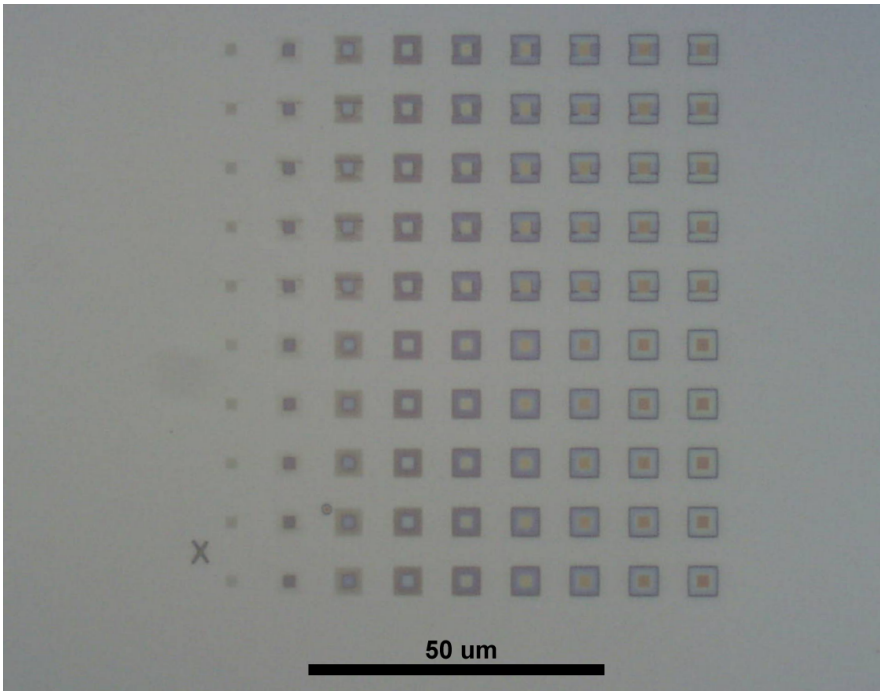

Figure 4.5 Optical micrograph demonstrating the polygon shifting problem displayed at 1000× magnification. The structures in the bottom 5 rows were created by exposing two rectangles, one inside the other. In the top five rows, the structures were created by exposing the central area with a higher dosage and surrounding it with 4 other polygons. As is visible, the polygons on either side have shifted slightly rightwards and upwards, creating gaps and overlaps of 250 nm.

and at times causing some polygons to shift, overlapping and over exposing some areas and leaving other areas unexposed, as shown in Figure 4.5. At even higher resolutions, the polygons sizes became as small as 2.5 pixel spacings - and it became unclear whether it would be exposed as 2 pixels or as 3. To counter this problem, patterns were then defined pixel by pixel, as the pattern generator placed pixels exactly where they were specified, regardless of any other settings. While it did correct the problem as desired, there were two disadvantages of doing this. The first was that the pattern file size grew enormously, and the second was that the inter-pixel beam settling time (which was the same as the inter-polygon settling time) caused exposure times to increase astronomically. This was countered somewhat by reducing the settling time between each pixel from 5 ms to 1 ms, with no observable decrease in pattern quality. Despite this, the settling time still accounted for around 90% of the total exposure time.

4.3.1.3 Development

Since ma-N2403 is not a chemically amplified resist, no post exposure baking was required before development. There were two developers available from the manufacturer [40] for the ma-N2403 resist - ma-D332 and ma-D532. They are both inorganic alkaline developers, but ma-D532 is the metal-ion-free (MIF) version. It was noted that the ma-D532 developer removed considerably more material than the ma-D332 developer

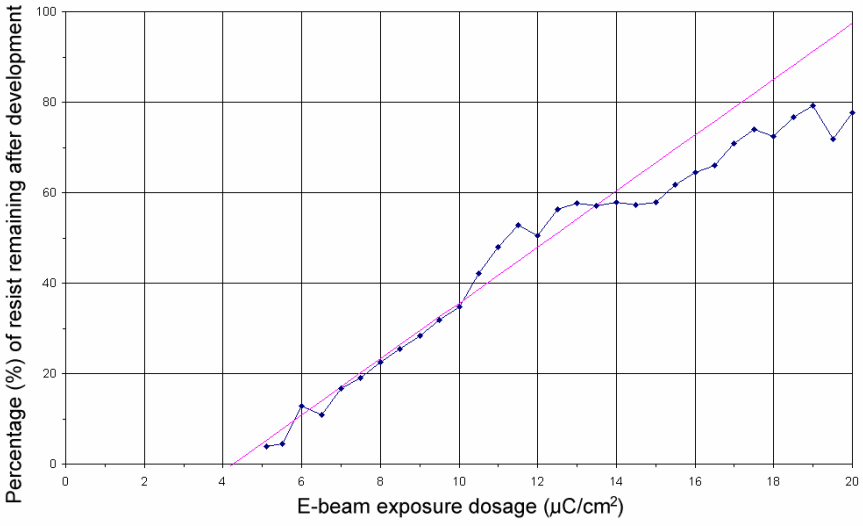

Figure 4.6 Contrast curve for large structures developed in the negative tone resist ma-N2403 written with an electron energy of 10 keV. The trend line shows the linearity of the resist between 5.0 μC/cm^2 and 15.0 μC/cm^2.

in the same time frame. This may have been due to the older age of the ma-D332 developer.

The ma-D332 developer was used for most of the work, as had already been characterised prior to obtaining the ma-D532, and since it took longer to develop, it meant it was easier to time accurately. It was found that the best development regime with ma-D332 was 30 s at room temperature (22 °C) followed by a 30 s rinse in DIW. The resist could easily be stripped with acetone.

Once a basic procedure had been developed, a dose test was performed with the pattern shown in Figure 4.4(a). After development, structure heights were measured by AFM, recorded and plotted creating the contrast curve shown in Figure 4.6. As can be seen, after around 15 μC/cm^2 the resist curve rolls off at 80 %. The curve however fails to show the quality of the structures, which declined from around 18 μC/cm^2 and higher dosages. This can be noted in the developed pattern by the scummy features appearing in the upper-right of Figure 4.7.

Figure 4.8 shows a optical micrograph of the developed resist after the New Zealand map shown in Figure 4.3 had been written. The image gained a 'Special art award' from Raith [42]. The pattern consisted of some 240,000 polygons and took 4 hours to write. It is envisioned with better beam control, allowing less settling time, and a faster pattern generator, the exposure time could be dropped to several minutes. The digital elevation model (DEM) data for the map was obtained from the USGS [46].

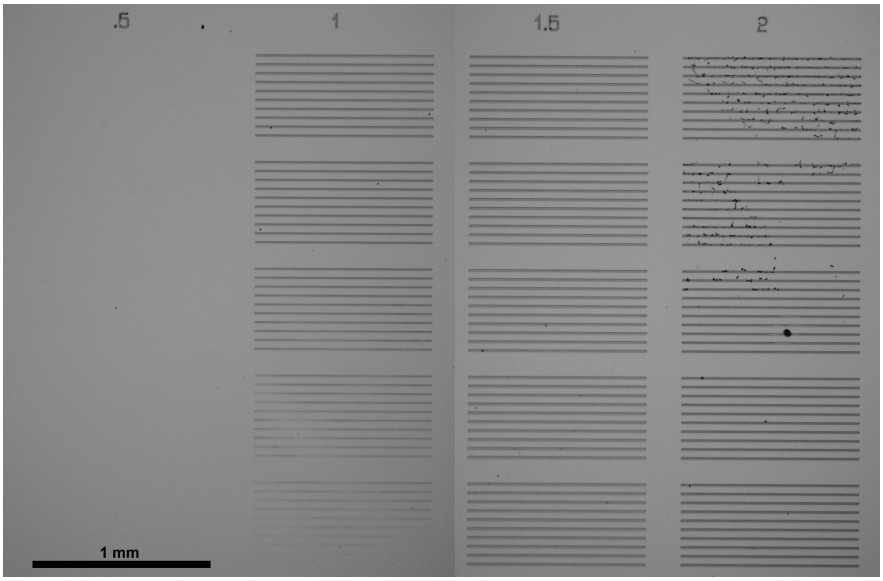

Figure 4.7 Optical micrograph of developed dose test. The dosages vary from 0.1 μC/cm^2 in the lower-left to 20.0 μC/cm^2 in the upper right. Visible in the upper-right is scum that remained attached to structures that had been exposed at 17.7 μC/cm^2 and above.

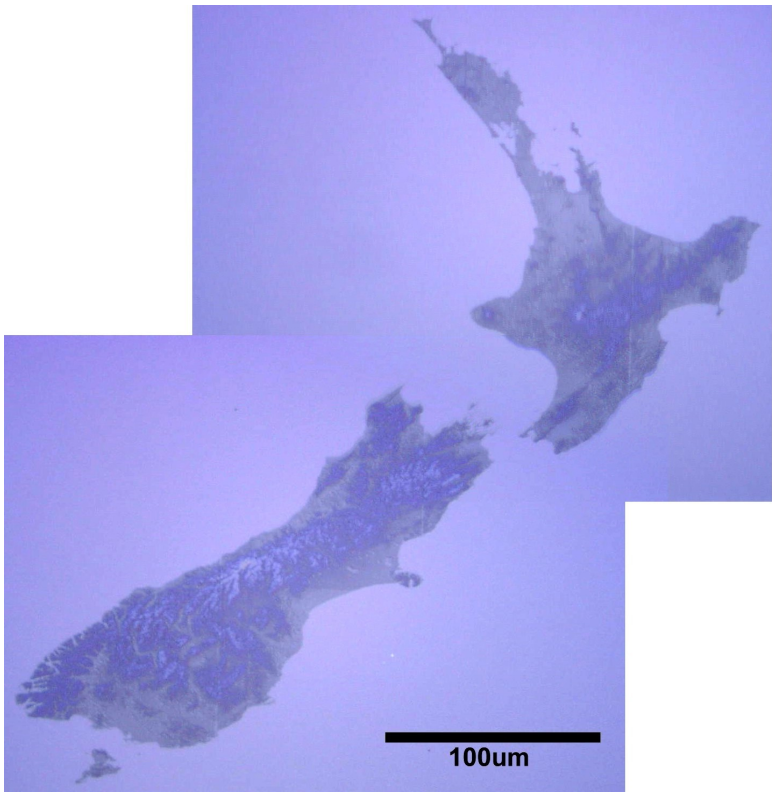

Figure 4.8 True colour optical micrograph of developed map of New Zealand. The scale of the map is 1:4,000,000,000. Different colours relate to different heights. The height was controlled by the exposure dosage, which varied between 5 μC/cm^2 for the low areas to 15 μC/cm^2 for the highest.

4.3.1.4 Reactive Ion Etching

Transferring the 3D patterns into the Si_xN_y substrate could only be performed by a single step reactive ion etch as illustrated in Figure 3.19. Other methods such as lift-off and indirect etch-back (Figures 3.17 and 3.18) can only work for 2D structures. Developing a good, reproducible procedure for transferring the pattern from the resist into the substrate required a large number of trails. RIE was exclusively used for this step and has a number of controllable variables which each can have a strong effect on the outcome. In the ideal situation the 3D structures in the resist would be transferred identically, except for a height multiplying factor. Several gas recipes were trialled in various ratios, flow rates, pressures and temperatures. The resist also played a part, and the ma-N2403 is described by the manufacturer as having 'excellent etch resistance in plasma processes'. The resist's etch selectivity was checked for several processes.

Before using the RIE machine, it was cleaned using a 20 minute oxygen, 200 W etch to remove contaminants from the chamber. Once this had been performed, the chamber was opened, sample loaded onto a nichrome coated electrode, and closed again inside a short time period. The chamber was then pumped down to at least 5×10^{-5} mbar, and cooled with liquid N_2 if required. All the gas lines to be used were then purged to ensure that no undesired residual gases from previous etches were present. Once the chamber pressure had once again dropped to 1×10^{-5} mbar, the desired gas bottles were opened, and correct flow rates set. When the gas flows had stabilised, the RF power was applied, and the etch began. When complete, the chamber was again pumped down to remove most etch by-products and bought back to room temperature. When the temperature was around 20 °C and all potentially harmful gases purged, the chamber was vented with N_2 and the sample unloaded and examined.

Three gas combinations in various ratios were used, and consisted of CHF_3/N_2, CHF_3/O_2 and CHF_3/Ar. In each case, CHF_3 was the primary gas which attacks the Si_xN_y substrate and the other gas used as a descummer. In the case of the CHF_3/N_2 gas combination, a pink plasma was noted, and all samples came out with pink coloured surface scum. It was determined that N_2 was unsuitable as a descummer. On the other hand, both Ar and O_2 worked well and had no visible residue on the samples post etching. To measure the etch rates of the resist and Si_xN_y substrates, a few samples were prepared with 3D structures, some of which had certain feature heights measured by AFM, giving H_I. The dry etch then took place, and the same structures were measured again, giving H_E. The remaining resist was then removed by ultrasonic bath in acetone, and the structures measured one final time, producing H_F. By using Equations 4.1 and 4.2 it is possible to work out the etch rates of both the resist and substrate.

$$EtchRate_{substrate} = \frac{H_F}{t} \tag{4.1}$$

Table 4.5 Reactive ion etch selectivities for three different gas combinations used to transfer 3D structures from ma-N2403 resist into a Si_xN_y substrate.

Process Parameter	Ar	O_2	N_2
Gas 1: flow rate (sccm)	(CHF_3) 27	(CHF_3) 25	(CHF_3) 25
Gas 2: flow rate (sccm)	(Ar) 21	(O_2) 5	(N_2) 10
Electrode type	Nichrome	Nichrome	Nichrome
Temp (K)	300	273	300
Time (min)	5	5	5
Etch pressure (mTorr)	20	20	20
H_I (nm)	250	310	295
H_E (nm)	350	310	290
H_F (nm)	150	250	140
Si_xN_y etch rate (nm/min)	30	50	28
Resist etch rate (nm/min)	10	50	29

$$EtchRate_{resist} = \frac{H_I + H_F - H_E}{t} \tag{4.2}$$

Etch processes and rates are shown in Table 4.5. The notable difference between Ar and O_2 etch processes was that while the process parameters were similar, the etch selectivities varied markedly, with the Ar etch having a notably higher selectivity, but lower etch rate. By using a combination of either 75 nm or 300 nm thick resist and either the O_2 or Ar etch recipes, it is possible to obtain Si_xN_y structures varying from 75 to 900 nm high.

It was decided to focus on use of the 75 nm thick resist due to reduced forward scattering and increased resolution, and the oxygen etch with a 1:1 etch selectivity to produce low structures for better mechanical strength. Since the molds would have low features, it also meant that they could be imprinted fully into the resist without the tallest mold structures hitting the target sample surface. To account for the reduced resist thickness and the desire to have no resist left post etch, the etch time was reduced to 2 minutes. At the 50 nm/min etch rate, this could remove up to 100 nm of resist meaning that all 75 nm of the low thickness resist would be removed, and allowed for some extra time if the plasma initially failed to strike. It would occasionally take up to 5 seconds for the plasma to strike. In later stages, the plasma failed to strike entirely, so the process was started at 40 mTorr, and lowered to 20 mTorr as soon as the plasma had struck. Once the etch had been completed, the samples were cleaned by acetone in the ultrasonic bath to remove any surface debris.

4.4 RESOLUTION ACHIEVED

This has been divided into two sections, one for the work done performed using PMMA as a resist, and the other using ma-N2403. For PMMA, both actual EBL resolution and

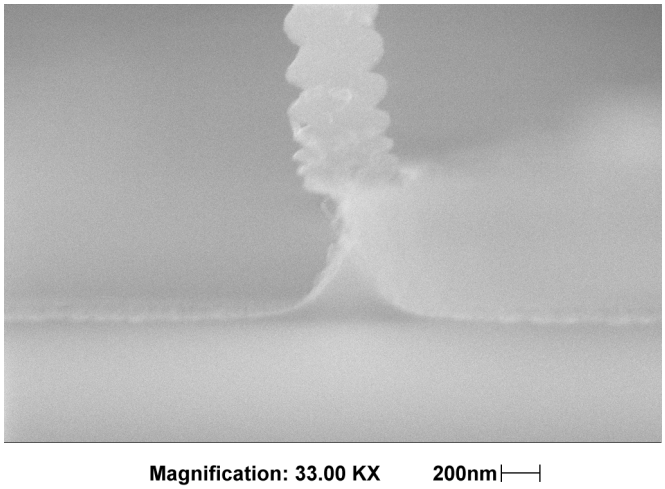

Figure 4.9 SEM view of a sectioned sample profile. The metal mask has detached from the other half of the section and can be seen curving upwards. The mask is 500 nm wide and has been thinned to a 20 nm wide structure with a RIE etch designed to undercut masks.

a thinning by RIE have been investigated. For the 3D resist, the maximum resolution under three different circumstances have been covered. This includes pillars on a raised structure, free standing pillars produced without height control and fine structures with height control.

4.4.1 2D Structures

With the older PSEM500, the system had a somewhat unstable beam control system that had a tendency to be under damped, which caused oscillations in which became apparent under high resolution inspection. Figure 4.9 shows by the wavy nature of the metal mask produced by lift-off. It shows that the pattern was written with a somewhat unstable beam, which was oscillating a distance 100 nm peak to peak. This pattern was written at higher beam current of 2,755 pA and a magnification of 640×. This effect became less noticeable with decreased beam current and higher magnification. For beam currents of 67 pA and a magnification of 10,000× the instability varied between 10 nm to 20 nm peak to peak.

The finest structures produced with the PSEM500 were 70 nm wide. Since they were not particularly fine structrues, it was decided to try thinning them during the dry etching process. To do this, a very reactive etch was used. This used SF_6 as the primary etching agent, along with O_2, higher etch temperatures and pressures. All the etches were performed with the same pattern, a group of 500 nm wide NiCr lines fabricated by EBL and lift-off. Every etch used the same nichrome electrode and 4 minute etch time. Table 4.6 shows some of the etches along with the lateral and vertical etch rates. As it can be noted, etches A through E use a gradually increased the SF_6 flow rate, and it can be noted that both the vertical and lateral etching increased. Progressing from

Table 4.6 Reactive ion etch recipes aimed to produce undercut profiles. All etches used the same 4 minute etch time and a nichrome electrode.

	Gas (sccm)		Temp	Pressure	Etch dist (nm)		Quality
	SF_6	O_2	(K)	(mTorr)	Undercut	Depth	
A	20	30	323	100	203	588	Profile ok, rough
B	40	30	323	100	244	649	Profile ok, rough
C	60	30	323	100	213	636	Smooth, 70° slope
D	80	30	323	100	234	677	20 nm wide, steep
E	100	30	323	100	>250	1,150	Undercut all the way
F	60	30	323	80	146	586	Profile ok
G	60	30	323	60	122	507	Rough, cavities
H	40	30	323	40	42	315	Smooth, steep edges
I	20	15	323	20	-23	230	Vertical, top overcut
J	60	30	173	100	56	461	Smooth and vertical

A to E, the structures got steeper and narrower until, in the case of E, so far undercut that the mask was totally detached from the substrate. The vertical etch rate was measured by the thickness of the remaining Si_xN_y layer and that subtracted from 2 μm. D had in effect the critical etch parameters - the structure was so thin, that when sectioned the metal mask remained in one piece and stayed attached to one half of the sample. This is visible in Figure 4.9. Other etches of note are shown in Figure 4.10. (a) was etched with recipe C in the Table 4.6. The 70° gradually gets steeper towards the top, while the open areas have been etched at a uniform rate. Structures (b) and (c) used recipes I and J respectively. (b) appears to be overcut, however it is more likely that the reactive nature of the etch has started etching the NiCr mask from the top and sides inwards, producing the visible structure. Other than that, the low pressure etch has produced a slight undercut with very steep and smooth sidewalls. (c) on the other hand has had an identical etch as (a), except the temperature was 173 K instead of 323 K. Due to the lower temperature, the ions had to provide more of the reaction energy, and most of these could only come from the plasma straight above the sample, meaning the etch would perform more anisotropically. As a result the etch rate was slower, and produced smoother structures.

4.4.2 3D Structures

Once the patterns were started being defined on a pixel-by-pixel basis, the true resolution of the ma-N2403 resist could be realised. Figure 4.11 (a) shows an AFM image of a 20×20 array of 90 by 75 nm pillars, with the central ones on a raised mesa. Each pillar is spaced at 250 nm. This was only the second scan to be performed with the tip, but due to the multiple sharp Si_xN_y features of the mold, the AFM tip was damaged very quickly and hence produced noticeable tip artefacts. A section through the AFM scan is shown in (b) where the pillars and raised mesa can clearly be seen.

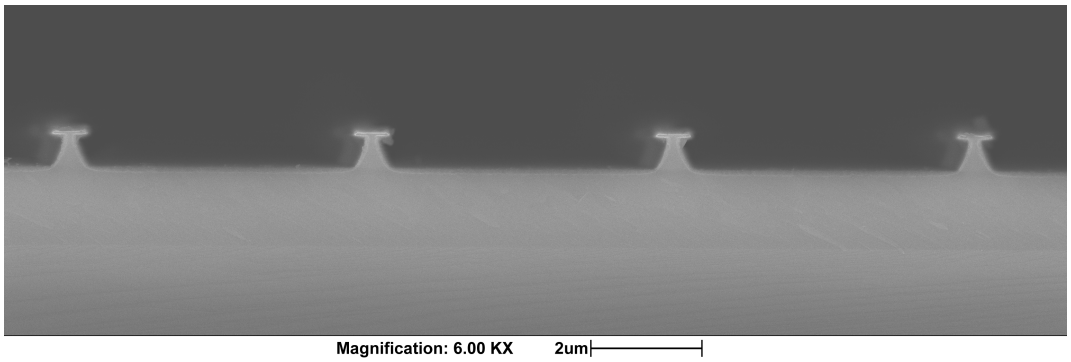

(a)

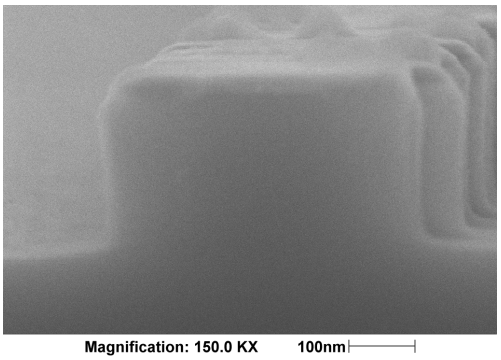

(b)

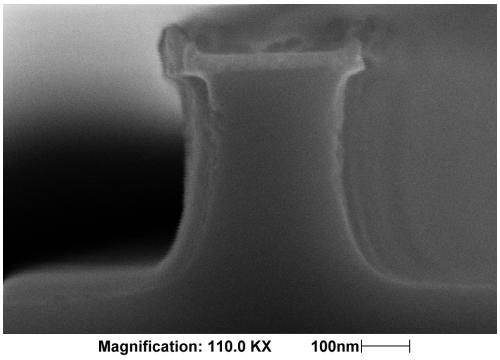

(c)

Figure 4.10 SEM micrograph of sectioned samples after being etched. (a) has been etched with high pressure, high flow, high temperature process. The boundary between the Si_xN_y and Si substrate can also be noted. (b) has been etched at lower pressure and gas flow rates, while (c) has been etched at a much lower temperature.

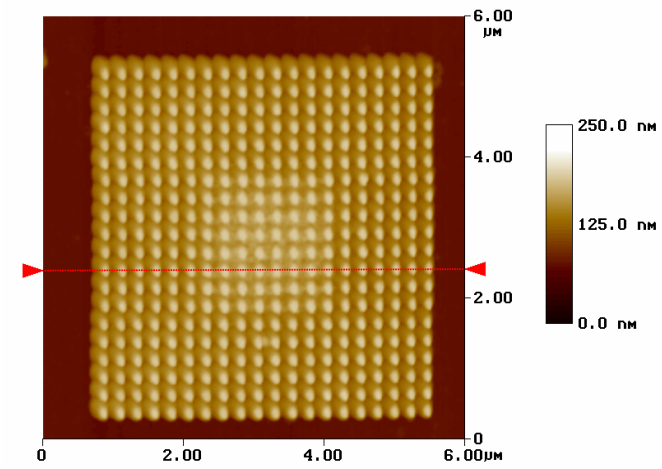

(a)

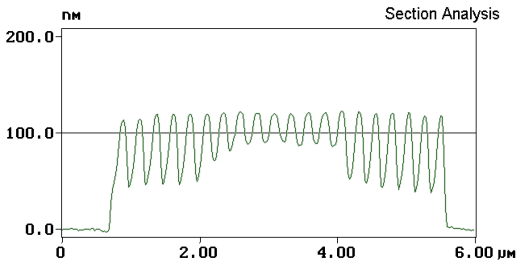

(b)

Figure 4.11 A AFM image (a) and section (b) of a 20×20 array of pillars. The pillars are 75 × by 90 nm, and the central pillars are on a raised mesa. The tip artefacts are due to the hard Si_xN_y mold damaging the AFM tip.

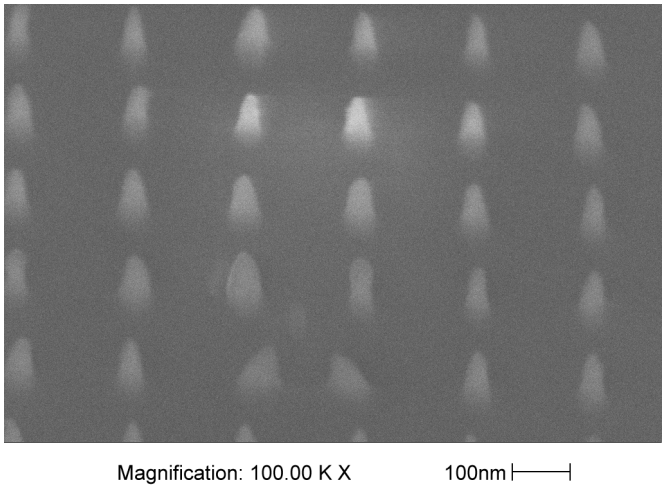

Figure 4.12 45° SEM image of pillars in ma-N2403 resist. The pillars are 100 nm high, with diameters ranging from 30 to 40 nm.

The highest resolution obtained with the ma-N2403 resist were pillars with a diameter between 30 and 40 nm, spaced as shown in Figure 4.12. The pillar height is also uniformly 100 nm, except for the two bottom central pillars. These appear to be leaning towards each other, and have a lower overall height than the others. This suggests that they have had the same exposure time as the other, except that the beam has moved during writing. This could be attributable to an electrical issue, but no source was found. The aspect ratio of the pillars is around 3:1, demonstrating the the resist has good potential for arbitrary sub 100 nm structures.

Control of fine feature height was also achieved, as illustrated Figure 4.13. Here the pattern consisted of three parallel lines of pixels, all spaced at 20 nm. The write dosage progresses from 1 μC/cm^2 to 20 μC/cm^2. However due to their very small structure size, any dosage below 12 μC/cm^2 failed to result in sufficient exposure of the resist. So for the lines visible in the image, the dosage linearly varied from 12 μC/cm^2 to 20 μC/cm^2, and corresponded in a very linear height increase from 8, 28, 30, 50, 48, 60, 71, 83 and 93 nm. The measured line widths varied from 80 nm to 94 nm, but includes the AFM tip diameter ($\sim$10 nm), so the actual widths are around 70 nm to 84 nm.

The finest period features produced with the resist was an array of pillars, spaced at 77 nm. However the maximum height differential of the gaps and the tops of structures was only 18.3 nm, whilst a difference around 10 nm occurred most often. Figure 4.14 shows a spectrum analysis of the shortest period.

4.5 SUMMARY

A number of aspects have been investigated for both 2D structures and 3D structures. For 2D structures these include developing controlled undercut etches that have been

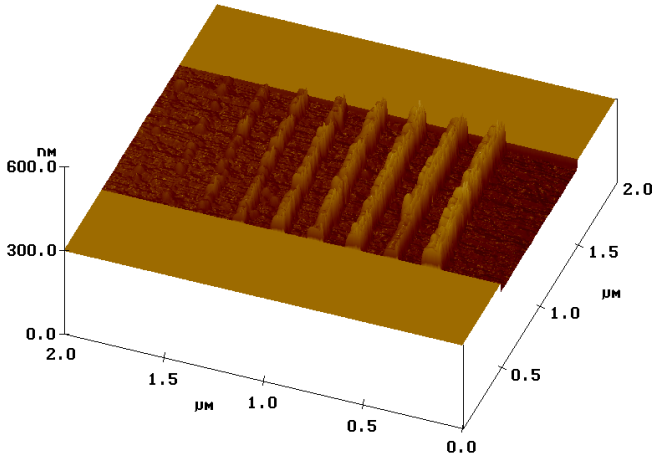

(a)

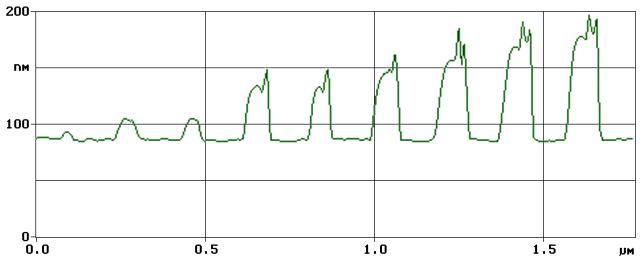

(b)

Figure 4.13 Sub 100 nm structures of controllable variable height. (a) is the 3D view of the AFM image, while (b) is a trace section through it. The structure heights varied linearly from 8 nm to 93 nm, while the structure widths vary between 80-94 nm wide.

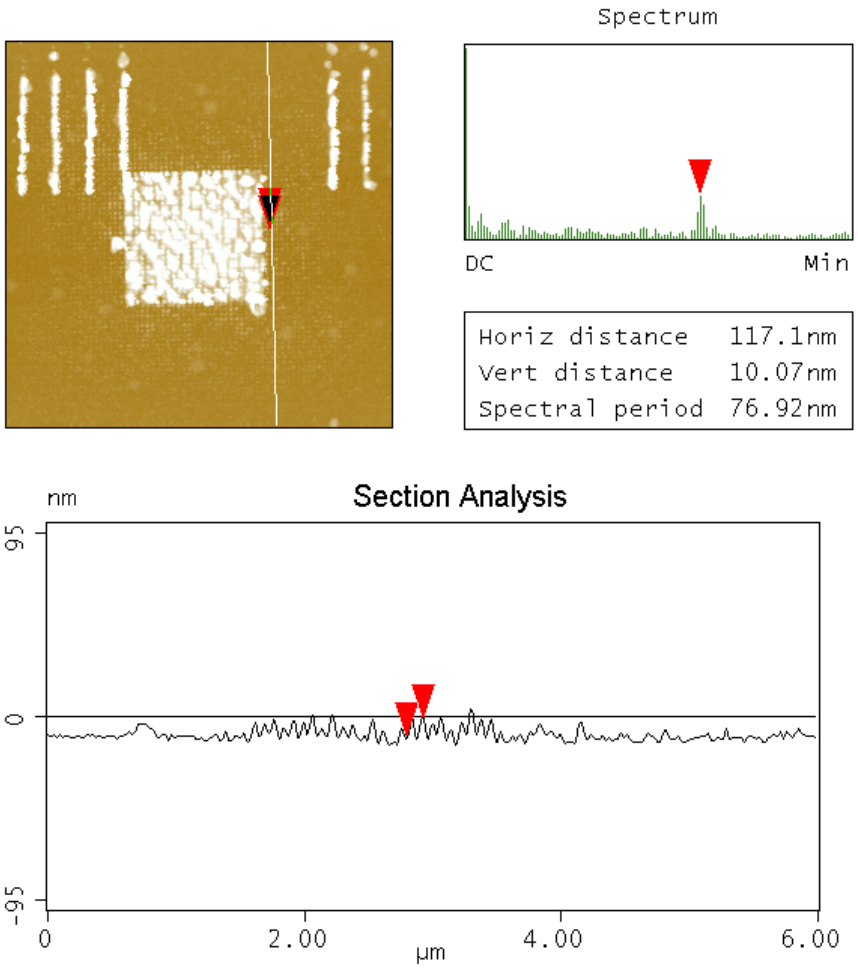

Figure 4.14 AFM image with cross section analysis. The shortest period achieved in the ma-N2403 resist was 77 nm, with an average height oscillation of 10 nm.

used to dramatically thin 500 nm features to only 20 nm. Other etches investigated are more suitable for applications with reduced lateral etch rates, producing deeper and steeper features.

For 3D structures various areas were investigated, covering the thinning, spin coating, pre-baking, lithography, development, and etch selectivities for the ma-N2403 resist. A reliable proceedure was found for all processes. A combination of two resist thicknesses and two of the developed etches, one with a selectivity of 1:1 and the other of 1:3, allowed for the fabrication of molds with feature heights varying between 5 nm and 900 nm. The resolution of the resist was also investigated, and the smallest features produced were 30 - 40 nm pillars that were 100 nm tall. The ability to linearly control the height of structures by varying the exposure dosage produced features between 4 to 93 nm tall at a width of no more than 84 nm. Sub 100 nm 3D structures, some on a raised mesa, were also patterned, showing that small 3D structures need not be free standing. The finest pitch realised was 77 nm, but only with height oscillation of 10 nm.

Chapter 5

IMPRINTING

5.1 OUTLINE

This chapter discusses the work performed directly relating to imprint itself. This includes the design and fabrication of an imprint press, the basics of low temperature imprint, methods of three-dimensional imprint, and results of imprints from a variety of patterns, thermal considerations, and lastly a brief investigation into anti-adhesion methods.

5.2 DESIGN OF IMPRINT PRESS

Part of the work performed involved designing and building an imprint press to replace the current equipment shown in Figure 3.20. This process began at the specifications that the new press would have to meet. This included being able to imprint at 100 bar across a 400 mm^2 sample at up to 120 °C with very reproducible results. This meant the system would require accurate monitoring of the temperature, pressure and time so that they could be automatically adjusted.

The final design allowed for automatic control of the heating time and temperature, but it was deemed that automatic control of the pressure would require too many moving parts and unnecessary complexities. Instead it was opted for an electronic pressure sensing system which would accurately report the force back to the user who could then adjust it as necessary. The design also included features that would allow the pressure to remain near constant through out the process without further input from the user.

Out of a number of requirements that were required to be met, a suitable design was developed. This is shown in Figure 5.1. The mold and samples is placed between the upper press plate (UPP) and the lower press plate (LPP). The 200 W cartridge heater is located inside the circular recess in the LPP, and a thermal transducer is located around to the right side. To apply pressure to the mold and sample, the screw is rotated anti-clockwise which moves the top pressure plate (TPP) down, compressing

the spring. This spring presses against the bottom pressure plate (BPP). By pulling down on L3, it exerts a force on fulcrum L2 at P4, which produces a 4 fold increase of force at P3, pushing the sliding press plate (SPP) downwards. By having L1 and L3 vertical, all lateral forces should be excluded from the imprint process, improving the imprint quality. However L1 and L2 are only perfectly vertical when the mold, resist and sample add up to a thickness of 1 mm. It will often be that it will be a few microns off, in which case all the points P1, P2, P3, P4, and P5 all have been pivoted and the SPP movement guided vertically by GR1 and GR2 to minimise any lateral forces. By having the spring located away from the heat source, its spring constant will not be affected by heating. This means that if the same spring compression is maintained that the pressure on the mold and sample would stay the same, irrespective of heating effects on others parts of the system. L2 also required extra engineering to ensure that it would not plastically deform (permanent shape change) during the harshest imprint process. The initial thickness estimate, of 24 mm, would have just withstood an imprint of 400 bar. By increasing the thickness by another 2 mm to 26 mm, the load strength of the beam before plastic deformation occurred was effectively quadrupled up to 1600 bar. It was decided to have a safety factor of only 4 otherwise the strain gauges mounted around P3 would be measuring very small amounts of flex and hence more susceptible to error.

The pressure can be measured either by foil strain gauges located in a bridge formation on both the front and back arms of L2 above and below P3, or by measuring the compression of the spring. As the pressure on the mold/sample increases, the lever arm L2 will bend slightly, making the top longer and bottom shorter, making a resistance differential in the foil gauges. This method is better suited for the micro controller to read in as it requires only some electronics and no extra moving parts. Measuring the compression of the spring is good for a rough visual verification of the pressure applied, but lacks precision as the spring is very stiff, and 1 mm difference in compression equates to roughly 60 bar difference in pressure on a 100 mm^2 sample. Foil strain gauges are more sensitive to heat than physical strain, so to prevent heat from effecting them the SPP has water cooling running continuously. This will balance the heat in L2 at both the bottom and top, meaning that the the surface temperatures where the foil gauges are mounted should be very similar and remain constant.

The temperature is monitored by a temperature controlled current device located on the right side of the LPP. The device allows one microamp of current per Kelvin to flow through it. This can easily be converted into a voltage by passing the current through a resistor, which is feed into one of the micro controllers ADC ports. The 200 W heater is mains powered and controlled by thyristors. The lower insulation block (LINS) is used to minimise heat loss from the LPP into the steel base plate. This layer consists of a 10 mm layer of Tufnol. This limits the thermal losses into the base plate to 7W when operating at 120 °C. The UPP has also been thermally isolated from the

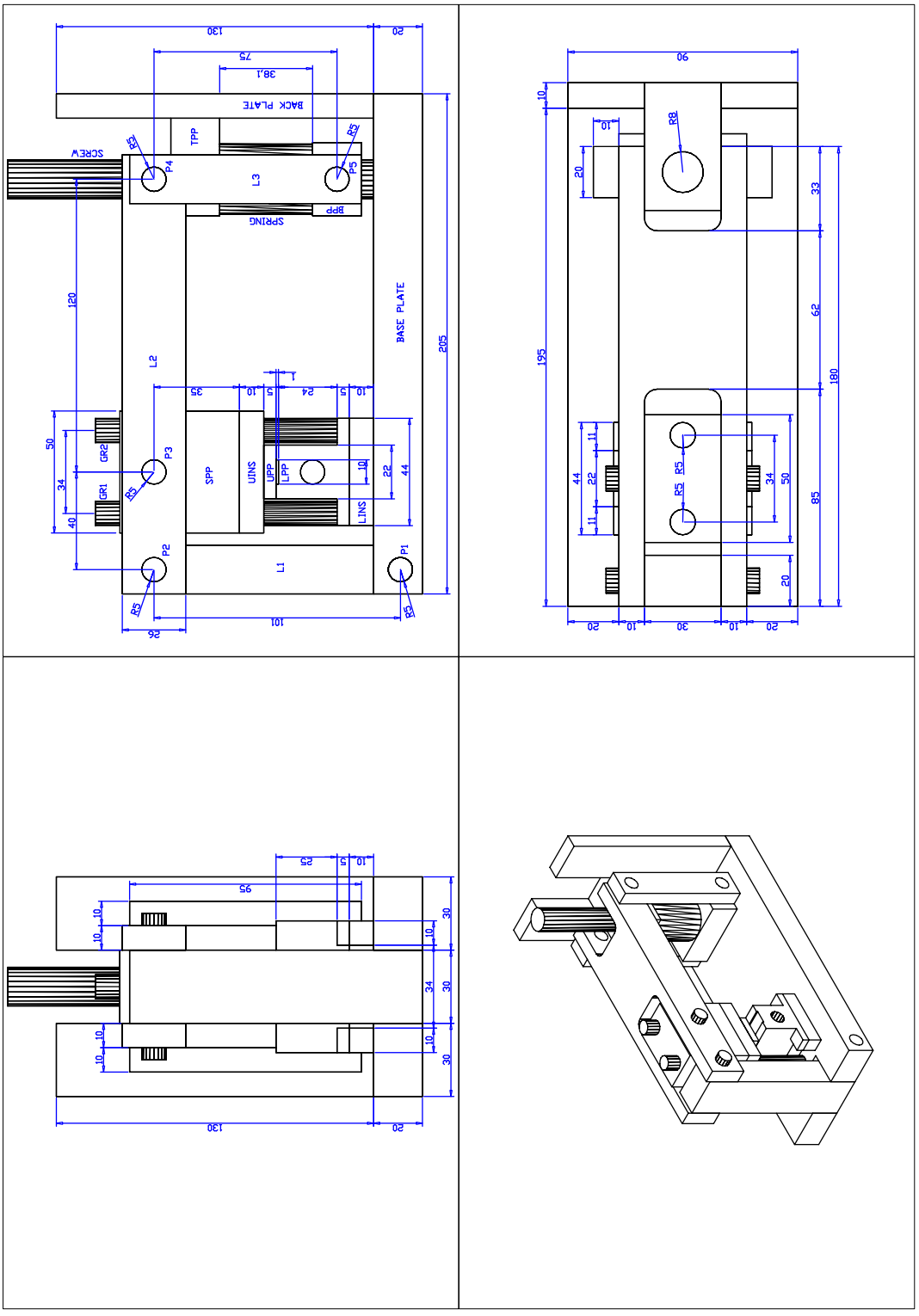

Figure 5.1 Technical drawings of designed imprint press. Going clockwise from top left is the Left view, Front View, Top view and 3D view looking from the top left front. The mold and sample are placed in the space between blocks marked UPP and LPP. The heater is located in the circular recess in LPP while the pressure is applied by turning the screw anticlockwise.

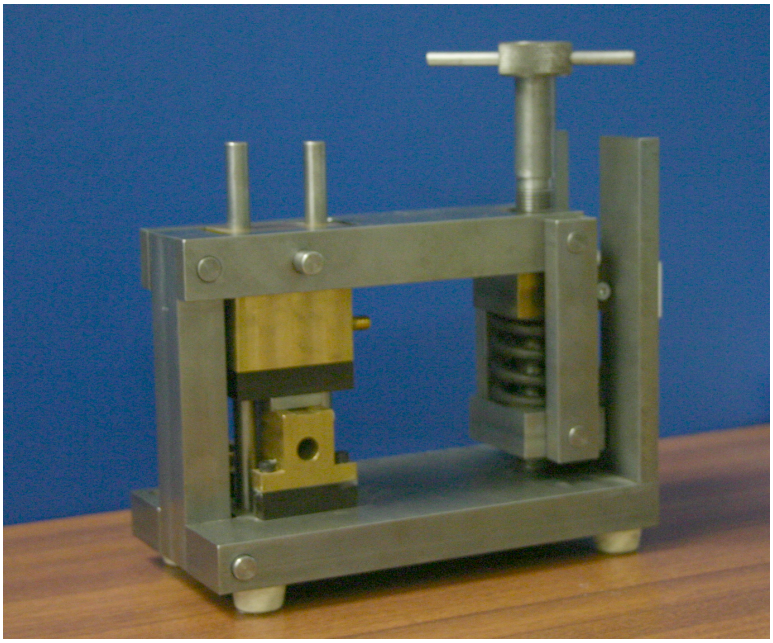

Figure 5.2 The new press built at the UoC. It is capable of providing up to 100 bar of pressure on to a 20 × 20 mm sample, and heating to 120 °C.

SPP by the upper insulation block (UINS), again 10 mm of Tufnol, but this has a lower loss due to the smaller surface area between the two layers. This loss is around 4 W at 120 °C. Thermal losses into the air will be minimal, so the total thermal loss of the system is near 12 W. Coupling this with the small thermal mass of the LPP and even smaller thermal mass of the UPP, the 200 W heater can easily and quickly heat the mold and sample. When the time has expired, the micro controller turns off the heater and turns on the water cooling for the LPP, to quickly cool the mold and sample.

Once the design of the press was completed, it was sent off to the departmental workshop to be built. The returned product is shown in Figure 5.2. During the construction of the press, the design and development of the electronics started. Special care had to be taken with the heater which run off mains power, due to it requiring a 230 V supply. The design resulted in the thyristor control being isolated from the micro controller by two opto-couplers, and all of the heater wiring shielded by ground wiring. By doing this and using a residual current device (RCD) to detect any current imbalance in the mains power supply, any dangerous electrical fault will very likely be shorted to a nearby ground resulting the the RCD tripping and isolating the fault. To further ensure the safety of the users, the heater wiring goes in one side of the LPP, while the water connectors are on the other, physically separating them should a water leak occur. The electrical schematic is shown in Figure 5.3. The power supply and mains zero crossing detection circuitry is shown in the top left, and immediately below it the thyristor firing circuitry. This circuitry has been designed such that the FIRE_P signal line must be pulsed, otherwise the thyristors will not fire. This is another safety

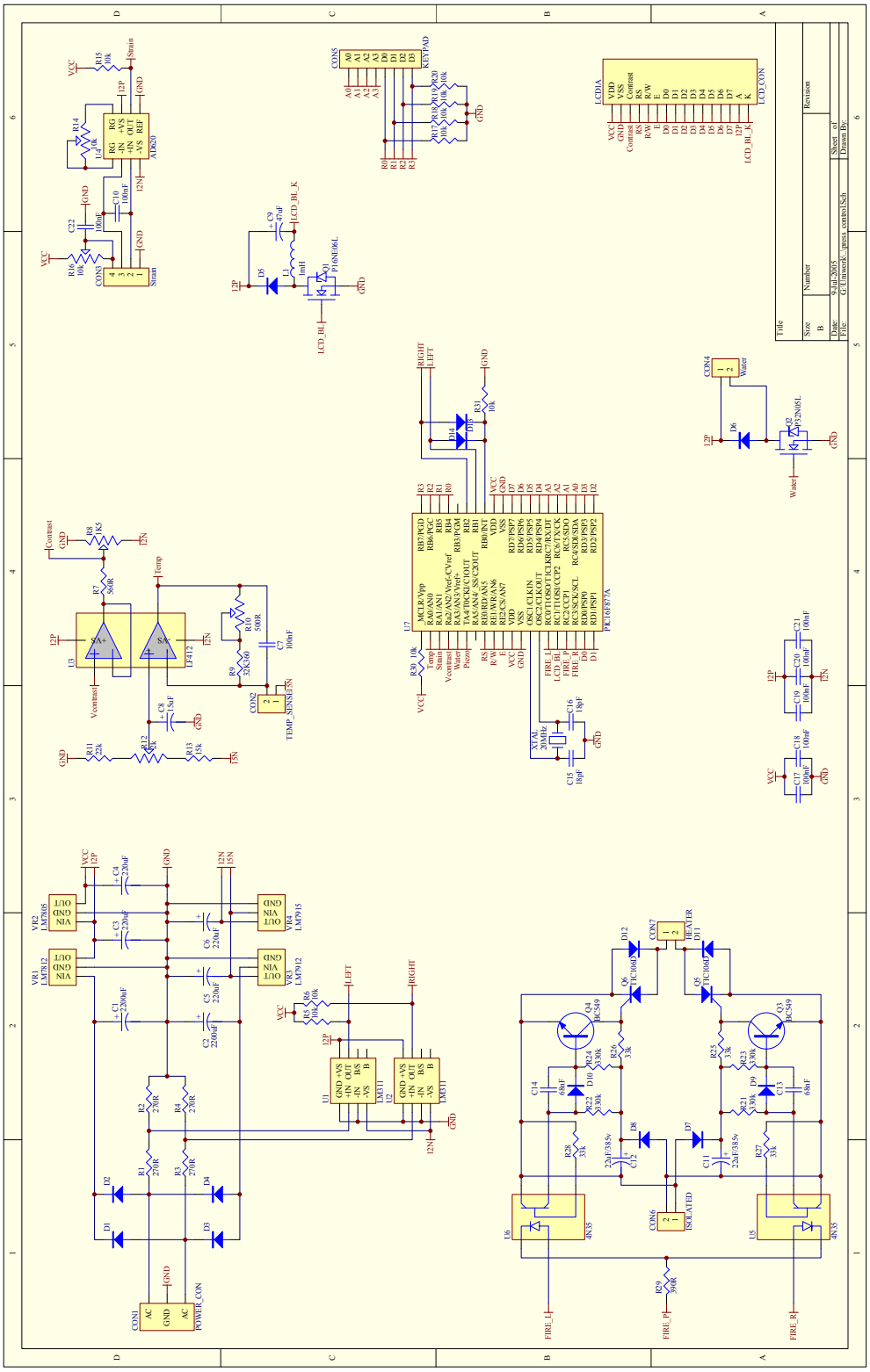

Figure 5.3 Schematic for imprint press controlling circuitry.

Table 5.1 Imprinting process parameters for imprinting into a single layer of LMW PMMA.

Pressure (bar)	100
Temperature (°C)	80
Time (min)	20
Quench Time (min)	2

measure to prevent the thyristors from becoming stuck permanently on should the micro controller freeze, preventing the heater from staying on full power. In the centre top is the temperature calibration circuit and contrast control for the LCD screen. On the top right is the strain gauge bridge calibration circuit and immediately below it the PWM control for the LCD back light. The next two parts downwards on the right is the keypad and LCD screen connectors respectively. In the centre is the micro controller with the reset and crystal set up, while below it is the decoupling capacitors and the cooling water valve controller.

Unfortunately, the imprint press did not became fully functional. While all mechanical functions did perform as desired, the heating control system was not fully calibrated, and the foil strain gauge bridge did not work as desired. The heating system relied on adjusting the firing angle of the thyristors to control the power output, the relationship between steady state temperature and firing angle was not obtained. This was necessary due to the delay between applying heat and the thermo-sensor registering the change. Pressure readings could not be accurately taken, as it strain gauge bridge gave inconsistent results between tests. Another issue was later discovered related to thermal expansion of the mold and sample and is discussed in Section 5.5.

5.3 LOW TEMPERATURE IMPRINTING PROCEDURE

While almost all studies have performed thermo-plastic imprinting between the T_G and T_D of the bulk material, few have performed it below the T_G. Previous research at the UoC [17, 1] have indicated that imprint may be performed below the glass transition temperature. It has been found for thin polymer films that the T_G is lower than that of the bulk material [39], and thus allowing lower temperature imprints.

The basic low temperature imprinting procedure was performed by pressing the mold into a single LMW PMMA layer on a Si substrate at a temperature below the T_g of the bulk material. The imprint conditions are shown in Table 5.1.

Preparation of the target substrate was performed by ultrasonically cleaning by immersion in acetone, methanol then IPA for five minutes each, and blown dry by N_2 gun after each step. To drive off any surface water they were dried at 185 °C in a convection oven for 30 minutes. Next, they were removed from the oven and allowed to cool to room temperature before being loaded into the spinner and having 2 drops of 4% LMW PMMA placed in the center and spun at 4000 RPM for 60 seconds. They

were then softbaked at 185 °C in a convection oven for 30 minutes to drive out the remaining solvent.

The only preparation the mold had to go through was cleaning. This was performed in the same fashion - acetone, methanol and IPA for 5 minutes each in the ultrasonic bath and dried at 185 °C. When both mold and target sample were ready, they were loaded into the imprint press with the target sample at the bottom facing upwards and the mold placed face down on top. A 10 × 10 mm piece of card was placed on top of the mold to absorb any high pressure points and ensure that a more uniform pressure was applied across the mold. The press was then tightened just enough so that the slack was removed from the spring. From here the required number of turns were taken to apply the desired pressure on the sample/mold combination. One 360° turn equated to an increase in pressure by 11 bar. The press was then placed on the hotplate which was already heated to the required temperature and the timer started. Once the time was up, the mold and sample were quenched by placing the entire press in a large beaker of DIW for 2 minutes. Once cool, everything was dried by N_2 gun, the press unwound and the mold and sample removed.

5.4 THREE-DIMENSIONAL IMPRINT LITHOGRAPHY

The major difference between imprinting '2D' and '3D' structures is down to the importance of structure height. The primary focus of 2D imprinting is to push the raised structures into the imprint medium and as close to the substrate as possible to transfer a binary pattern. In general the deeper the trenches between raised areas on the mold, the better as it gives space for resist to flow to. Aside from that and the mechanical strength of the mold, there is no special requirements for the feature height. For 3D structures, the height of structures is critical and should be accurately reflected in the imprinted result. The first part is making sure that the mold feature heights meet requirements, and the second the imprinting requirements. There are three methods to ensure the imprint does go to the right depth, as illustrated in Figure 5.4. The first is to use an absolute measuring system and record how far apart the mold and sample are and press to the correct distance. This method would be beneficial for use, however the hardest to implement. The second method the imprints occurs as deep as possible, so that there are no voids between the mold and resist. The third option is to have raised features placed at regular intervals on the mold to act as spacers during imprint to ensure the mold can go up to, but no further than the desired distance in to the resist.

Each system has its own advantages and disadvantages. The second method was intended as the exclusive use in this study as it places no special requirements on either mold or substrate, and does not require special equipment. The only requirement is that the resist thickness needs to be at least as great as the highest feature on the mold.

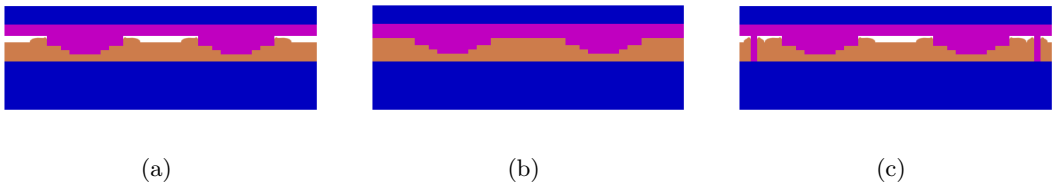

(a) (b) (c)

Figure 5.4 Methods of controlling imprint depth for 3D structures. (a) uses an accurate controller to measure and limit the depth of imprint, (b) imprints full depth so that there is no free space between mold and sample, and (c) uses spacers placed at regular positions to limit the imprint depth.

The major disadvantage with this system is the amount of resist reflow that needs to occur to fill all the voids if large structures are being imprinted.

Imprinting the mold shown in Figure 4.11 produced informative results. The conditions of imprint were as those specified in Table 5.1. It was found that the pattern was accurately reproduced, illustrated in Figure 5.5. However the pillars were taller than the resist was thick, effectively performing a 3D imprint shown in Figure 5.4 (c). The pillars prevented the raised mesa from being imprinted to the full depth, but due to the resist reflowing around it, it has still left an impression. It can also be noted in the image that the imprinting itself did not occur in a perfectly vertical fashion, as the resist reflow is higher on the lower right corners of structures. This indicates a movement of the mold during imprint in that direction. Further information is available by looking at the cross sectional view, where it can be noted that the central pillars have not imprinted to the full depth. This is not due to the mold, but bowing. Bowing occurs when sufficient resist cannot flow away from a tall structure, and happens most often with large structures that are imprinted to the full depth of the resist. Other factors can also effect this, including imprint pressure, temperature, time and resist viscosity. In this case it has been caused by a combination of the raised mesa, the pillars, and high resist viscosity. The pillars prevent the resist from flowing easily, and the raised mesa tries to push large volumes of resist away. Elastic deformation occurs, and when the pressure is removed, and the resist relaxes back into a less stressed state. The easiest solution to this problem would be to use a lower viscosity imprint medium.

The 3D map of New Zealand (Figure 4.8), was also used in imprint. Using the standard parameters described in Table 5.1, the process worked very well, illustrated in Figure 5.6. The minimum feature size on the pattern is 250 nm squares, which are observable in both the mold and imprint. Here it is also noticeable that the imprint did not occur to full depth. This can be seen by a slight halo outlining the imprinted image where the mold and sample lost contact. Where structures (mountains) were imprinted, the halo is further from the edge of the pattern, but closer near laterally protruding features. This is also visible in the AFM image of both the mold and imprinted pattern in Figure 5.7.

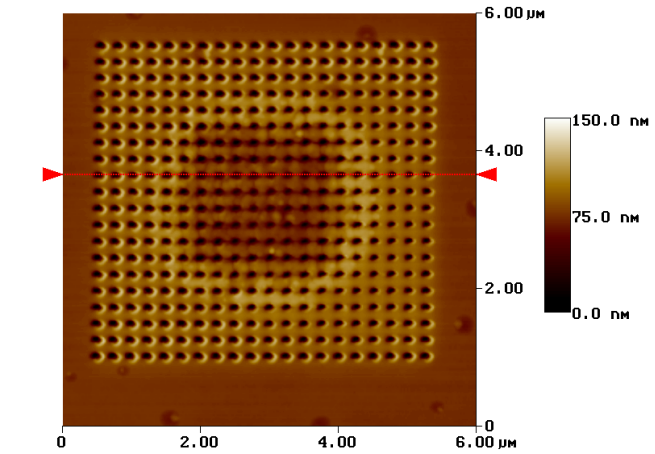

(a)

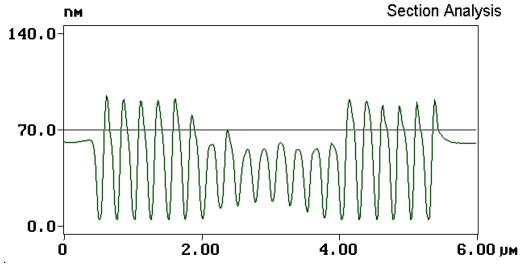

(b)

Figure 5.5 Imprinting of a three-dimensional mold. (a) AFM image of pattern imprinted into PMMA at 80 °C. (b) Cross section of AFM image, the pillars and platform can clearly be seen recessed into the PMMA, as well as the upwards bowing of the resist in the middle.

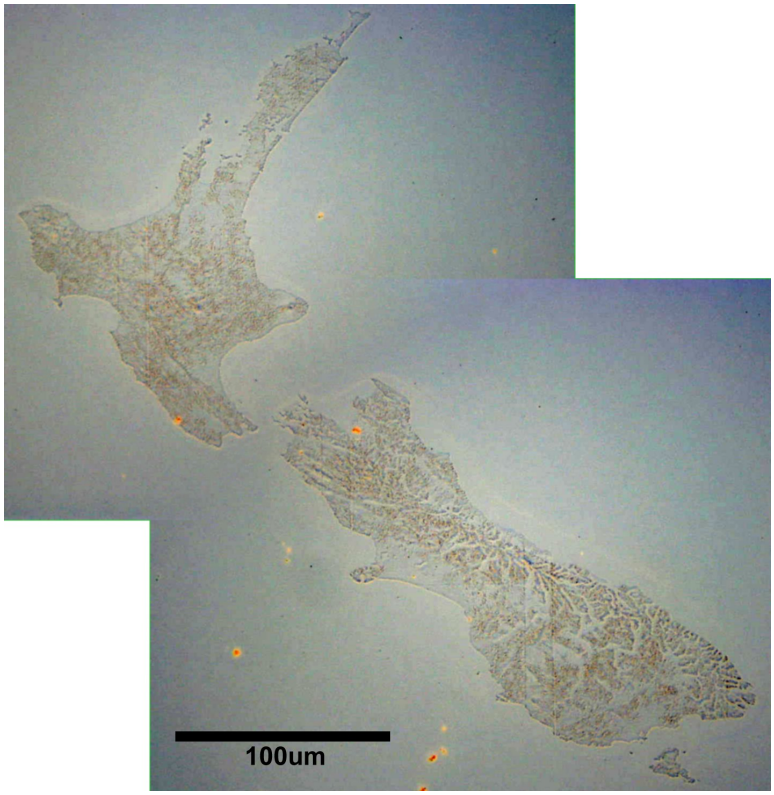

Figure 5.6 Optical micrograph of 3D map of New Zealand imprinted in to PMMA below the bulk glass transition temperature.

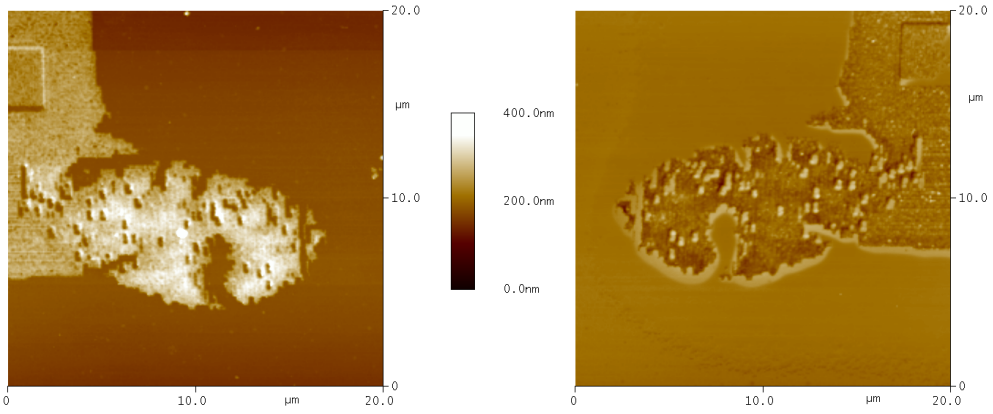

(a) (b)

Figure 5.7 AFM image of mold (a) and imprint (b) of a 3D map of New Zealand. It can be noted by presence of reflowed resist that mold has not been imprinted to full depth. Near the bottom and left edges of the image, it is possible to observe the point where the mold and sample lost contact on the flat surfaces.

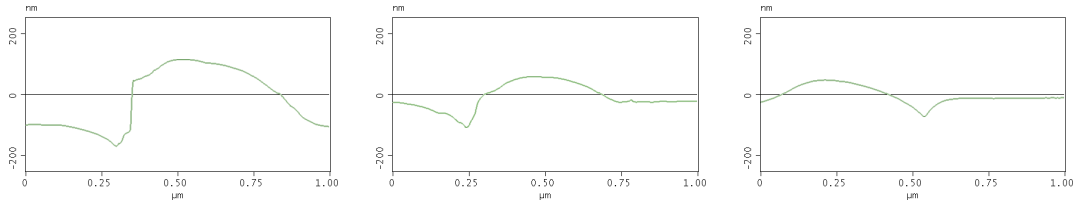

(a) (b) (c)

Figure 5.8 AFM traces of trenches imprinted into PMMA. Trace (a) was taken on the left side of the sample, (b) near the centre and (c) on the right side. This indicates that the target sample has thermally expanded more than the mold has during imprint.

5.5 THERMAL EXPANSION

As discussed in detail in Section 2.2.1, thermal expansion needs to be taken into account. It was noted with the imprinted patterns that the resist reflow tended to come out on a single side of a pattern. When looked at on a larger scale, a trend was noticed. Generally all the reflow moved towards the centre point of the sample, indicating that it was not the fault of the mold moving, but rather a difference in thermal expansion between the mold and sample. To confirm this hypothesis, the sample shown in Figure 4.9 was stripped of the metal layer, cleaned and imprinted, producing the results illustrated in Figure 5.8. Here it is clear that it is the case that resist has flowed towards the centre. The difference in thermal expansion cannot be put down to the Si_xN_y substrate, as it is only a 2 μm film coated onto an ordinary Si substrate. This means that both the mold and sample will have the same thermal expansion coefficient. Therefore, only a temperature imbalance can be causing this this problem.

There are two possible times for this imbalance to occur; the first is during the initial heating, and the second during quenching. It would seem unlikely to occur during cooling, as both the mold and sample will be cooling at very similar rates and temperatures, as the entire press being placed in DIW water. However, on the heating cycle, the thermal energy enters through the bottom of the press, heating the base, then sample, then mold and finally the top half of the press. Due to the relatively low thermal conductivity of the mold/sample combination and the relatively high thermal mass of the upper part of the press, most of the temperature difference will occur across the mold/sample. This will cause the sample to expand faster than the mold making it appear that the reflow occurs towards the centre. If the mold was on the bottom, the resist reflow would be outwards from the centre due to the mold expanding faster than the sample.

A method to correct this problem is to heat the entire press up to the required temperature before loading the mold and sample and performing the imprint. This has been performed with the same mold as for the previous imprint, and the results are shown in Figure 5.9. The cooling cycle for this imprint was left as per the standard procedure. Here it is noticeable that there is considerably less bias in the direction of

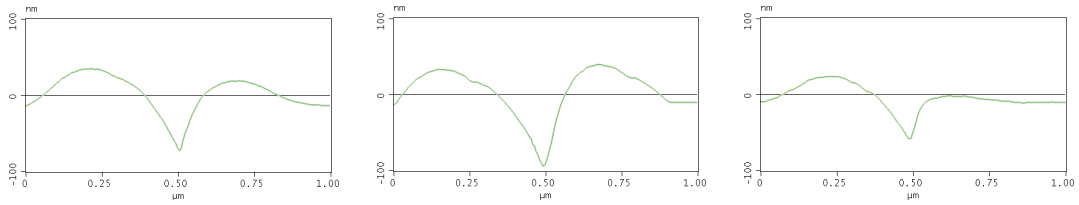

(a) (b) (c)

Figure 5.9 AFM traces of trenches imprinted into PMMA with the revised process. Trace (a) was taken on the left side of the sample, (b) near the centre and (c) on the right side. From these three traces we can determine that there is no trend of resist flowing towards or away from the centre, but there is a slight bias towards to left.

resist flow, supporting the hypothesis that the uneven heating of the mold and sample caused the reflow towards the centre.

5.6 ANTI-STICK COATINGS

While it has been reported that lower temperature imprints reduce the sticking problem [47], and the procedure described so far produced good results, occasionally the mold would stick to the imaging layer, and when removed pull some of the resist off. To counteract this problem it was decided to test some methods to prevent sticking. The methods reviewed can be divided into two main categories, the first by applying some release agent before imprint which would reduce adhesion between mold and resist, and the second surface treating the mold surface to prevent adhesion.

MRA, the release agent tried was a food grade polymer which is used in food industry to prevent sticking between mold and plastic trays which were being molded. This was applied to the target sample prior to imprint by placing one small drop ($\sim$10 μL) on the surface. The mold was then placed on top and it was found that due to the surface tension between the release agent and both the mold and sample that the two parts lined up with each other. This combination was then placed in the press and imprinted. While some of the pattern did transfer, the release agent film was so thick that in places prevented any imaging occurring. Figure 5.10 shows both the mold and sample after imprint. As is visible, the mold had residual release agent on it, and would require cleaning before the next imprint could occur. This is not desirable in industry as it would significantly slow down the process. The target sample on the other still had large amounts of release agent on the surface. Even if the polymer had been thinly applied, it still would have left residue on the mold, making it unsuitable for NIL.

Another method looked into, but not tested was the use of a TiO_2 coating over the mold. TiO_2 is a very strong and non-stick coating which is commercially used in a number of industries. However to coat the mold uniformly in a very thin layer it would require either Ti evaporation from a omnidirectional source so that vertical surfaces could be coated, then oxidate the surface, or a chemical vapour deposition (CVD)

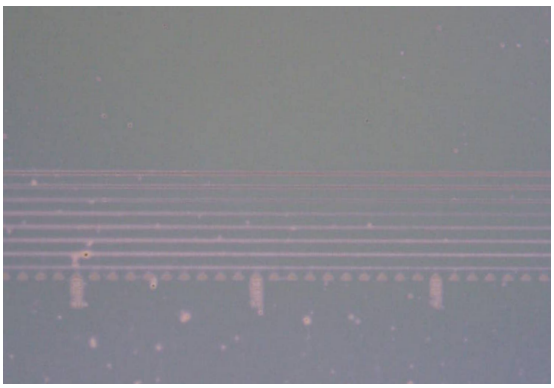

(a)

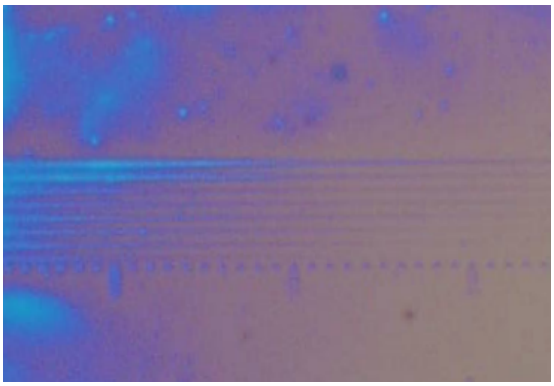

(b)

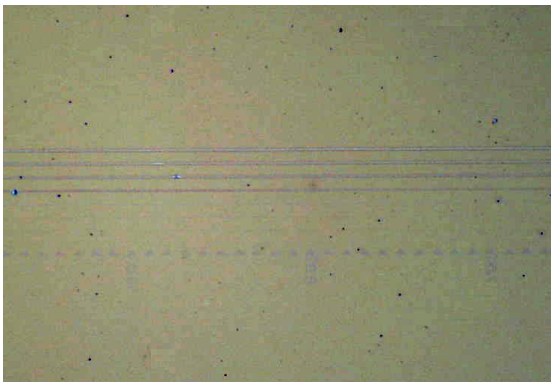

(c)

Figure 5.10 Optical images of mold (a) and sample (b) post imprint using MRA, a food grade release agent. Part (c) shows a prior imprint without the use of MRA.

method. Uniform evaporation of Ti was not possible as the UoC evaporator did not have a rotating stage holder. CVD was briefly investigated, however after observing some zirconia deposition and the principals behind it, and the difficulty in creating fully dense films [48] it was decided that it was beyond the scope of this study.

The final method investigated was the use of a fluoro-silane to treat the surface. Fluoro-silianes covalently bond to the substrate as described in Section 2.2.5, and are capable of with standing temperature, pressure, most bases and acids, and is a very thin coating. For this study some FOTS ($CF_3(CF_2)_5(CH_2)_2SiCl_3$) was purchased from Gelest [49]. For silanes to react with the surface, water needs to be present to help the reaction. To ensure the molds had a water film on the surface prior to treating with FOTS, the samples were loaded into a 100% humidity chamber for 20 minutes. The humidity chamber consisted of a large sealable vessle with DIW heated to 30 °C in the bottom, with a mesh platform above it, on which the molds were placed. During this time the FOTS solution was prepared. This consisted of adding 10 mg of FOTS to 10 ml of dry n-heptane. The samples were then submerged in the solution for a period of time between 1 and 3 minutes. When removed from the solution, all the liquid ran off, leaving a dry surface. To ensure the FOTS had covalently bonded with the substrate, the samples were annealed on a hotplate at 120 °C for 20 minutes. One sample did not get treated properly, and this was noted for having water droplets on the surface prior to being placed in FOTS, and on removal from the solution it still had droplets. These may have been water, but it was not possible to confirm.

To test the effectiveness of the FOTS treatment, the molds were all tested in the imprint process. The standard parameters as per Table 5.1 were used. In the normal procedure with untreated samples, the mold and sample usually required gentle pulling to separate them. In contrast, the treated samples simply came apart when removed from the press. No quantifiable measurements were taken as the forces required to separate them were too minute. However, two positive indications what the treatment worked were noted. The first thing noted is that when rinsed in DIW, all the water ran straight off, leaving the mold surface dry, indicating a hydrophobic surface. Secondly, and more importantly, it was found that no further sticking occurred during imprint.

5.7 SUMMARY

This chapter has provided detail on the imprint work performed. This includes design and construction of an imprint press, 3D imprinting techniques, imprinting results including sub-100 nm resolution features, and issues relating to bowing, thermal expansion and sticking.

The press was designed prior to the investigation into the problems with thermal expansion, and so does not take into account the possibility of the sample expanding

slower or faster than the mold. However, the problem should be solvable with some modifications to the press.

Although one methodology of 3D imprinting was attempted, the mold feature heights were too high and another was performed instead. However, imprinting of 3D structures was still successfully performed into PMMA at temperatures below the glass transition temperature of bulk PMMA. Three issues with imprinting were noted however. The first was that of bowing, which was not corrected, but can be by performing imprint into a less viscous material. The second was that of thermal expansion, which was fixed by preheating the press before loading the mold and sample. The final issue was that of sticking, while only happening occasionally, was still a cause for concern. By treating the surface with a low energy fluoro-silane, further sticking problems were prevented.

Chapter 6

CONCLUSIONS AND FUTURE WORK

6.1 CONCLUSIONS

The study reported in this thesis investigated the fabrication of nanoimprint lithography molds and then their use in pattern replication. The fabrication covers the resist coating, e-beam lithography, reactive ion etching. The imprinting covers the design of an imprint press, imprinting, thermal considerations, and anti-stick coatings.

In the fabrication of the molds, the initial work was performed producing 2D structures on the older PSEM500. A reactive ion etch recipe was developed to thin these structures, and in one case a reduction from a 500 nm wide mask to a 20 nm wide line was achieved. Further work was then performed adjusting the techniques learnt for producing 2D structures for fabricating 3D structures, and involved the characterisation of the ma-N2403 resist. This included thinning the resist down and spin coating it on 75 nm thick, addressing the lack of adhesion of small resist structures to the SiN substrate by using HMDS, electron beam lithography and finding the contrast curve. Further work was also performed developing two reactive ion etches, one with a 1:1 selectivity that uses a CHF_3/O_2 gas combination and the other 1:3 using CHF_3/Ar, to transfer the structures into the SiN substrate. These were low pressure etches intended to transfer the patterns into the resist without the thinning of features. Etches involving the use of CHF_3/N_2 did not work well as large polymer build-ups occurred during etching. With the refining of the EBL procedure by specifying the pattern pixel-by-pixel and reducing the beam current, high resolution features were also created in the 3D resist. This includes the fabrication of features with periods down to 77 nm, 100nm high pillars that with sub-40 nm diameters, and sub-90 nm wide lines with heights variably controlled between 5 to 93 nm.

On the side of imprinting, a number of areas were investigated. The advantage and disadvantages of several imprinting methods were discussed in Chapter 2. An imprint press was designed and built. This failed to work as desired due to a lack of characterisation of the heating system and difficulties in getting the pressure measurement system to work well. It was also discovered later that the press would also be

affected by thermal expansion problems, when the mold and sample expand at different times causing uneven resist reflow. The molds were successfully imprinted into PMMA at temperatures below the glass transition temperature of the bulk material, with no damage observed. This included 2D and 3D structures with no deterioration in the reproduced patterns, except for when the mold failed to imprint to full depth due to it hitting the substrate. Difference in thermal expansion was also investigated and a method found to reduce its effect. Anti-adhesion coatings were also investigated and a mold treatment with FOTS eliminated any further sticking problems.

Most of the fabrication methods investigated in this study can be directly transferred to fabrication of molds from different materials, such as quartz, where the mold can be used in step and flash imprint lithography. Minor changes might need to be performed to the RIE recipes so as to obtain a suitable selectivity, but the rest of the procedures should not require any changes. By using SFIL, pattern replication will become easier as UV curable monomers can be dispensed in the required amounts and are very fluid allowing for room temperature, low pressure imprint, which would resolve several issues outlined in this thesis.

6.2 FUTURE WORK

With SFIL the most likely candidate, in the authors opinion, to succeed as the NGL, it is important that the maximal benefit is obtained from the potential of relatively simple and cheap 3D lithography. However, before this can happen there is an important area in 3D NIL that requires more research, and that is the manner in which the imprint depth is controlled. Whilst the methods used in Figure 5.4 outline how it might be done, more analysis needs to be done determining what technique is best for what application. For instance in the imprinting of lenses, it would seem that full depth imprint is the only manner which is appropriate. For this technique to work well, it seems reasonable that a low viscosity medium would be required, and that the correct amount is accurately applied. For other purposes, using pillars as spacers would fit the requirement nicely for performing 3D lift-off, as described in the next section.

6.2.1 3D lift-off

A new method has been envisioned to create metal interconnect layers using two different imprinting methods. This method would produce a via layer and one interconnect layer with one mold, effectively eliminating half of the metal layer interconnect alignment steps. This is demonstrated in Figure 6.1. A sample is ready for the next layer of processing (a). Firstly SOG or HSQ is applied (b) and flash imprinted (c). The mold is removed (d), and a break through etch is performed (e). A clean substrate is prepared with a resist for inking (f), reverse imprinted (g), leaving only resist on

structures that have been contacted (h). Metal evaporation is performed (i), followed by lift-off (j). Another dry etch is performed (k) to level the top of the substrate (l). The small remaining voids can be filled in with the next process step.

SOG and HSQ both have low dielectric constants, act as planarisers when spin-coated, are currently used to fill the areas between interconnects, and can be UV cured, making them an ideal medium to perform SFIL into. This method will also work well for producing T-gate transistors directly onto the substrate.

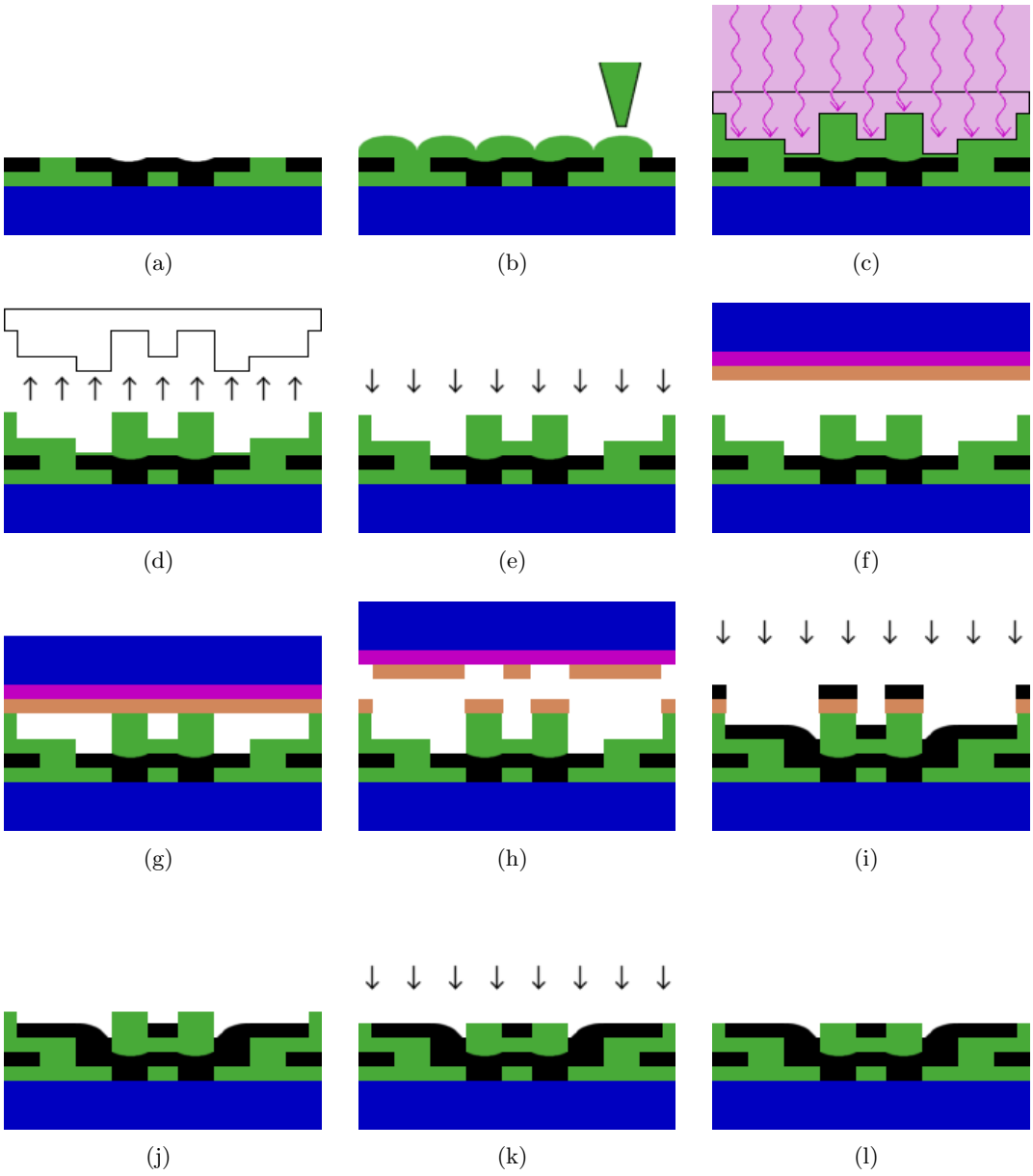

Figure 6.1 An envisioned scheme for producing 3D metal interconnect layers by lift off.

Appendix A

AUTHORS PUBLICATIONS

A.1 AUTHORED

A.1.1 Microelectronic Engineering (2005)

M. Konijn, M.M. Alkaisi, R.J. Blaikie, 'Nanoimprint Lithography of Sub 100-nm 3D Structures,' *Microelectronic Engineering*, vol. 78-79, pp. 653-658, 2005.

A.1.2 AMN2 Poster (2005)

M. Konijn, M.M. Alkaisi, R.J. Blaikie, 'Fabrication of 3D Nanoimprint Lithography Molds,' *International Conference on Advanced Materials and Nanotechnology*, Poster Section SL-P3, see Figure A.1.

A.2 CO-AUTHORED

A.2.1 Current Applied Physics (2004)

M.M. Alkaisi, W. Jayatissa, M. Konijn; 'Multilevel Nanoimprint Lithography,' *Current Applied Physics*, vol. 4, no. 2-4, pp. 111-114, 2004.

A.3 PRESENTATIONS

M. Konijn, 'Sub-100 nm 3D e-beam lithography,' Raith users meeting, Rotterdam, The Netherlands, September 2004 during the Micro and nano engineering conference.

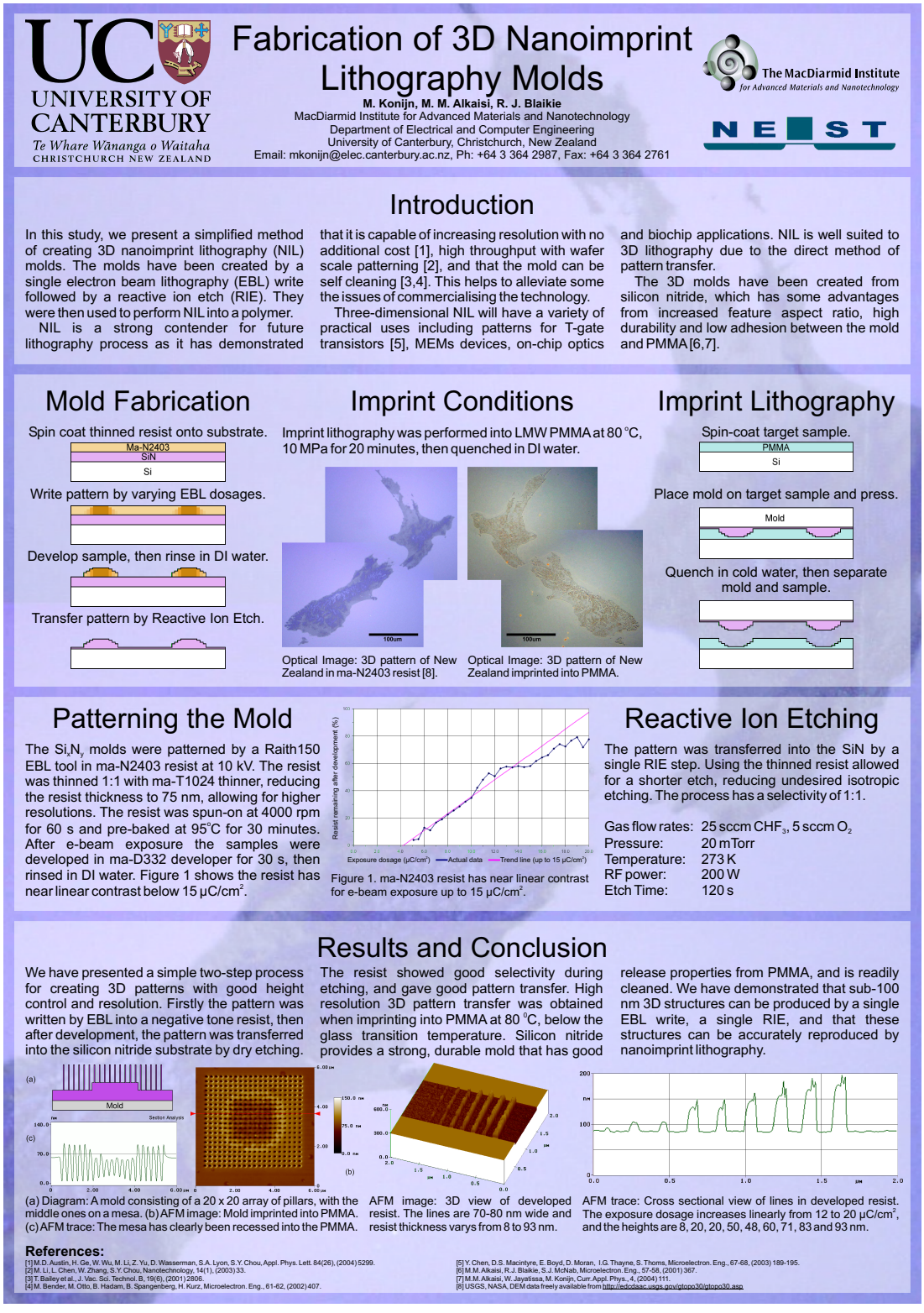

Figure A.1 Poster presented at the Second International Conference on Advanced Materials and Nanotechnology, 2005, Queenstown, New Zealand.

REFERENCES

[1] C. A. N. W. Jayatissa, "Nanostructure engineering by means of nanoimprint lithography," Masters dissertation, University of Canterbury, 2003.

[2] Y. Chen, D. Macintyre, E. Boyd, D. Moran, I. Thayne, and S. Thoms, "Fabrication of high electron mobility transistors with t-gates by nanoimprint lithography," in *Papers from the 46th International Conference on Electron, Ion, and Photon Beam Technology and Nanofabrication*, vol. 20. Anaheim, California (USA): AVS, 2002, pp. 2887–2890.

[3] D. J. Resnick, S. Sreenivasan, and C. G. Willson, "Step & flash imprint lithography," *Materials Today*, vol. 8, no. 2, pp. 34–42, 2005.

[4] *Molecular Imprints*, 2005, http://www.molecularimprints.com/.

[5] K. A. Lister, S. Thoms, D. S. Macintyre, C. D. W. Wilkinson, J. M. R. Weaver, and B. G. Casey, "Direct imprint of sub-10 nm features into metal using diamond and sic stamps," in *The 48th International Conference on Electron, Ion, and Photon Beam Technology and Nanofabrication*, vol. 22. San Diego, California (USA): AVS, 2004, pp. 3257–3259.

[6] M. D. Austin, H. Ge, W. Wu, M. Li, Z. Yu, D. Wasserman, S. A. Lyon, and S. Y. Chou, "Fabrication of 5 nm linewidth and 14 nm pitch features by nanoimprint lithography," *Applied Physics Letters*, vol. 84, no. 26, pp. 5299–5301, 2004.

[7] S. Y. Chou, P. R. Krauss, and P. J. Renstrom, "Imprint of sub-25 nm vias and trenches in polymers," *Applied Physics Letters*, vol. 67, no. 21, pp. 3114–3116, 1995.

[8] G. E. Moore, "Cramming more components into integrated circuits," *Electronics*, vol. 38, no. 8, 1965.

[9] J. H. Burnett, Z. H. Levine, and E. L. Shirley, "Intrinsic birefringence in crystalline optical materials: A new concern for lithography," *Future Fab Intl*, vol. 12, 2002.

[10] B. Fay, "Advanced optical lithography development, from uv to euv," *Microelectronic Engineering*, vol. 61-62, pp. 11–24, 2002.

[11] R. Menon, A. Patel, D. Gil, and H. I. Smith, "Maskless lithography," *Materials Today*, vol. 8, no. 2, pp. 26–33, 2005.

[12] B. Mertens, M. Weiss, H. Meiling, R. Klein, E. Louis, R. Kurt, M. Wedowski, H. Trenkler, B. Wolschrijn, and R. Jansen, "Progress in euv optics lifetime expectations," *Microelectronic Engineering*, vol. 73-74, pp. 16–22, 2004.

[13] J. Feeney, "The economic imperative behind progress," *Future Fab Intl*, vol. 18, 2005.

[14] S. Park, H. Schift, C. Padeste, B. Schnyder, R. Kotz, and J. Gobrecht, "Anti-adhesive layers on nickel stamps for nanoimprint lithography," *Microelectronic Engineering*, vol. 73-74, pp. 196–201, 2004.

[15] M. Keil, M. Beck, T. G. I. Ling, M. Graczyk, L. Montelius, and B. Heidari, "Development and characterization of silane antisticking layers on nickel-based stamps designed for nanoimprint lithography," *Journal of Vacuum Science & Technology B: Microelectronics and Nanometer Structures*, vol. 23, no. 2, pp. 575–584, 2005.

[16] H. Lee and G. Jung, "Wafer to wafer nano-imprinting lithography with monomer based thermally curable resin," *Microelectronic Engineering*, vol. 77, no. 2, pp. 168–174, 2005.

[17] M. M. Alkaisi, R. J. Blaikie, and S. J. McNab, "Low temperature nanoimprint lithography using silicon nitride molds," *Microelectronic Engineering*, vol. 57-58, pp. 367–373, 2001.

[18] U. Plachetka, M. Bender, A. Fuchs, B. Vratzov, T. Glinsner, F. Lindner, and H. Kurz, "Wafer scale patterning by soft uv-nanoimprint lithography," *Microelectronic Engineering*, vol. 73-74, pp. 167–171, 2004.

[19] W. M. Choi and O. O. Park, "A soft-imprint technique for submicron-scale patterns using a pdms mold," *Microelectronic Engineering*, vol. 73-74, pp. 178–183, 2004.

[20] M. Bender, U. Plachetka, J. Ran, A. Fuchs, B. Vratzov, H. Kurz, T. Glinsner, and F. Lindner, "High resolution lithography with pdms molds," in *The 48th International Conference on Electron, Ion, and Photon Beam Technology and Nanofabrication*, vol. 22. San Diego, California (USA): AVS, 2004, pp. 3229–3232.

[21] M. Otto, M. Bender, F. Richter, B. Hadam, T. Kliem, R. Jede, B. Spangenberg, and H. Kurz, "Reproducibility and homogeneity in step and repeat uv-nanoimprint lithography," *Microelectronic Engineering*, vol. 73-74, pp. 152–156, 2004.

[22] S. Y. Chou, P. R. Krauss, and P. J. Renstrom, "Nanoimprint lithography," in *The 40th international conference on electron, ion, and photon beam technology and nanofabrication*, vol. 14. Atlanta, Georgia (USA): AVS, 1996, pp. 4129–4133.

[23] H. Lee and G. Jung, "Full wafer scale near zero residual nano-imprinting lithography using uv curable monomer solution," *Microelectronic Engineering*, vol. 77, no. 1, pp. 42–47, 2005.

[24] C. Perret, C. Gourgon, F. Lazzarino, J. Tallal, S. Landis, and R. Pelzer, "Characterization of 8-in. wafers printed by nanoimprint lithography," *Microelectronic Engineering*, vol. 73-74, pp. 172–177, 2004.

[25] X. D. Huang, L.-R. Bao, X. Cheng, L. J. Guo, S. W. Pang, and A. F. Yee, "Reversal imprinting by transferring polymer from mold to substrate," in *Papers from the 46th International Conference on Electron, Ion, and Photon Beam Technology and Nanofabrication*, vol. 20. Anaheim, California (USA): AVS, 2002, pp. 2872–2876.

[26] L.-R. Bao, X. Cheng, X. D. Huang, L. J. Guo, S. W. Pang, and A. F. Yee, "Nanoimprinting over topography and multilayer three-dimensional printing," in *Papers from the 46th International Conference on Electron, Ion, and Photon Beam Technology and Nanofabrication*, vol. 20. Anaheim, California (USA): AVS, 2002, pp. 2881–2886.

[27] K.-i. Nakamatsu, K. Watanabe, K. Tone, H. Namatsu, and S. Matsui, "Nanoimprint and nanocontact technologies using hydrogen silsesquioxane," *Journal of Vacuum Science & Technology B: Microelectronics and Nanometer Structures*, vol. 23, no. 2, pp. 507–512, 2005.

[28] S. Matsui, Y. Igaku, H. Ishigaki, J. Fujita, M. Ishida, Y. Ochiai, H. Namatsu, and M. Komuro, "Room-temperature nanoimprint and nanotransfer printing using hydrogen silsequioxane," *Journal of Vacuum Science & Technology B: Microelectronics and Nanometer Structures*, vol. 21, no. 2, pp. 688–692, 2003.

[29] S. Matsui, Y. Igaku, H. Ishigaki, J. Fujita, M. Ishida, Y. Ochiai, M. Komuro, and H. Hiroshima, "Room temperature replication in spin on glass by nanoimprint technology," in *The 45th international conference on electron, ion, and photon beam technology and nanofabrication*, vol. 19. Washington, DC (USA): AVS, 2001, pp. 2801–2805.

[30] T. Bailey, B. Smith, B. J. Choi, M. Colburn, M. Meissl, S. V. Sreenivasan, J. G. Ekerdt, and C. G. Willson, "Step and flash imprint lithography: Defect analysis," in *The 45th international conference on electron, ion, and photon beam technology and nanofabrication*, vol. 19. Washington, DC (USA): AVS, 2001, pp. 2806–2810.

[31] H. Lee, "Effect of imprinting pressure on residual layer thickness in ultraviolet nanoimprint lithography," *Journal of Vacuum Science & Technology B: Microelectronics and Nanometer Structures*, vol. 23, no. 3, pp. 1102–1106, 2005.

[32] M. J. Pellerite, E. J. Wood, and V. W. Jones, "Dynamic contact angle studies of self-assembled thin films from fluorinated alkyltrichlorosilanes," *J. Phys. Chem. B.*, vol. 106, no. 18, pp. 4746–4754, 2002.

[33] J.-K. Chen, F.-H. Ko, K.-F. Hsieh, C.-T. Chou, and F.-C. Chang, "Effect of fluoroalkyl substituents on the reactions of alkylchlorosilanes with mold surfaces for nanoimprint lithography," in *The 48th International Conference on Electron, Ion, and Photon Beam Technology and Nanofabrication*, vol. 22. San Diego, California (USA): AVS, 2004, pp. 3233–3241.

[34] K. A. Lister, B. G. Casey, P. S. Dobson, S. Thoms, D. S. Macintyre, C. D. W. Wilkinson, and J. M. R. Weaver, "Pattern transfer of a 23 nm-period grating and sub-15 nm dots into cvd diamond," *Microelectronic Engineering*, vol. 73-74, pp. 319–322, 2004.

[35] H. Ooe, M. Morimatsu, T. Yoshikawa, H. Kawata, and Y. Hirai, "Three-dimensional multilayered microstructure fabricated by imprint lithography," *Journal of Vacuum Science & Technology B: Microelectronics and Nanometer Structures*, vol. 23, no. 2, pp. 375–379, 2005.

[36] W. Wu, J. Gu, H. Ge, C. Keimel, and S. Y. Chou, "Room-temperature si single-electron memory fabricated by nanoimprint lithography," *Applied Physics Letters*, vol. 83, no. 11, pp. 2268–2270, 2003.

[37] H. J. Levinson, *Principles of lithography*, ser. SPIE Press monograph ; PM97. Bellingham, Wash.: SPIE Press, 2001.

[38] *Laurell Technologies Corporation*, 2005, http://www.laurell.com/.

[39] J. A. Forrest, K. Dalnoki-Veress, J. R. Stevens, and J. R. Dutcher, "Effect of free surfaces on the glass transition temperature of thin polymer films," *Phys. Rev. Lett.*, vol. 77, no. 10, pp. 2002–2005, 1996.

[40] *Micro Resist Technology*, 2005, http://www.microresist.de/.

[41] L. de Broglie, *Recherches sur la thorie des quanta*. Paris,: Masson, 1924.

[42] *Raith*, 2005, http://www.raith.com/.

[43] *Oxford Instruments*, 2005, http://www.oxfordplasma.de/.

[44] *BOC Edwards*, 2005, http://www.bocedwards.com/.

[45] K. R. Williams and R. S. Muller, "Etch rates for micromachining processing," *Journal of Microelectromechanical Systems*, vol. 5, no. 4, pp. 256–269, 1996.

[46] *U.S. Geological Survey*, 2005, http://edcdaac.usgs.gov/gtopo30/gtopo30.asp.

[47] N. Lee, Y.-K. Kim, and S. Kang, "Temperature dependance of anti-adhesion between a stamper with sub-micron patterns and the polymer in nano-moulding processes," pp. 1624–1629, 2004.

[48] S. Krumdieck and R. Raj, "Growth rate and morphology for ceramic films by pulsed-mocvd," *Surface and Coatings Technology*, vol. 141, no. 1, pp. 7–14, 2001.

[49] *Gelest*, 2005, http://www.gelest.com/.